Neutral pion and η meson production at midrapidity in Pb-Pb collisions at $\sqrt{s_{NN}} = 2.76$ TeV

S. Acharya *et al.**
(ALICE Collaboration)

(Received 21 March 2018; published 4 October 2018)

Neutral pion and η meson production in the transverse momentum range $1 < p_T < 20$ GeV/c have been measured at midrapidity by the ALICE experiment at the Large Hadron Collider (LHC) in central and semicentral Pb-Pb collisions at $\sqrt{s_{NN}} = 2.76$ TeV. These results were obtained using the photon conversion method as well as the Photon Spectrometer (PHOS) and Electromagnetic Calorimeter detectors. The results extend the upper p_T reach of the previous ALICE π^0 measurements from 12 to 20 GeV/c and present the first measurement of η meson production in heavy-ion collisions at the LHC. The η/π^0 ratio is similar for the two centralities and reaches at high p_T a plateau value of $0.457 \pm 0.013^{\text{stat}} \pm 0.018^{\text{syst}}$. A suppression of similar magnitude for π^0 and η meson production is observed in Pb-Pb collisions with respect to their production in pp collisions scaled by the number of binary nucleon-nucleon collisions. We discuss the results in terms of Next to Leading Order (NLO) pQCD predictions and hydrodynamic models. The measurements show a stronger suppression than observed at lower center-of-mass energies in the p_T range $6 < p_T < 10$ GeV/c. For $p_T < 3$ GeV/c, hadronization models describe the π^0 results while for the η some tension is observed.

DOI: 10.1103/PhysRevC.98.044901

I. INTRODUCTION

Quantum chromodynamics (QCD) [1], the fundamental theory of strong interactions, predicts that, above a certain critical energy density, hadrons melt into a quark-gluon plasma (QGP) [2,3]. Such a state of matter is believed to have existed a few microseconds after the Big Bang [4]. One of the goals of lattice QCD calculations is the understanding of the properties of strongly interacting matter and the nature of the phase transition that depends on the values of the quark masses and number of flavors. For vanishing baryon chemical potential (μ) and for quark masses above a critical quark mass, a deconfinement transition associated with chiral restoration takes place through a smooth crossover [5–8]. The study and characterization of the QGP gives information on the crossover transition as well as insights on the equation of state of deconfined matter [9,10]. These transitions are expected to have occurred in the early universe and therefore their study is also of relevance to cosmology [4].

Heavy-ion collisions at relativistic energies offer the possibility of studying the QGP by creating systems of dense matter at very high temperatures. Of the many observables that probe the QGP, measurements of π^0 and η meson production over a large transverse momentum (p_T) range and in different colliding systems are of particular interest. At low p_T ($p_T < 3$ GeV/c), light meson production in heavy-ion collisions gives insights about hadronization and collectivity in the evolution of the QGP. At high p_T ($p_T > 5$ GeV/c), it helps quantify parton energy loss mechanisms [11,12]. High-p_T particle suppression in heavy-ion collisions with respect to pp collisions may be modified by cold nuclear matter effects, such as nuclear parton distribution function (nPDF) modifications with respect to the vacuum. Measurements in pA collisions are thus needed to disentangle cold nuclear effects from the observed high-p_T particle suppression in AA collisions.

Other interesting probes of the QGP that can benefit from neutral meson measurements are studies of direct photon and heavy-flavor production measurements [13,14]. The π^0 and η mesons are the two most abundant sources of decay photons (and electrons); as a consequence, they generate the primary background for these rare probes. The first measurement of direct photons at the Large Hadron Collider (LHC) [15] employed m_T scaling and the K^0_s reference measurement to estimate the η contribution to decay photons. Forthcoming direct photon and heavy-flavor measurements at the LHC will be able to use the η measurement directly.

Measurements of pion spectra at Relativistic Heavy Ion Collider (RHIC) [16,17] at low transverse momentum were observed to be well described by thermal models that assume a hydrodynamic expansion of a system in local equilibrium [18]. The comparison of these models to data suggested the presence of a thermalized system of quarks and gluons formed in the early stages of the collision. At LHC energies, the thermal models that describe the RHIC data also describe the ALICE charged pion spectrum [19] for $p_T > 0.5$ GeV/c. Modern versions of these models fold in their calculations hydrodynamic expansion, which accounts for transverse flow effects, simultaneous chemical, and thermal freeze-out and inclusion of high mass resonance decays from the PDG [1].

*Full author list given at the end of the article.

Among the many models that aim at explaining low-p_T particle production, the equilibrium and chemical nonequilibrium statistical hadronization models (EQ SHM and NEQ SHM, respectively) have had their validity tested against LHC data from $p_T > 0.1$ GeV/c. The physics picture behind the NEQ SHM is a sudden hadronization of the QGP that leads to the apperance of additional nonequlibrium chemical potentials for light and strange quarks. The low-p_T pion enhancement predicted by the NEQ relative to the EQ SHM can be interpreted as the onset of pion condensation in ultrarelativistic heavy-ion collisions at the LHC energies [20–24]. Both predictions can be further tested by measuring π^0 and η production at LHC energies.

In the early RHIC program, a suppression of high-p_T π^0 production was observed in heavy-ion collisions when compared to scaled pp data [25]. This suppression was interpreted as a consequence of the energy loss of the scattered partons in the QGP generated in the collisions. From these observations, it was deduced that the dense QGP medium is opaque to energetic (hard) colored probes. Regarding high-p_T particle production at the LHC, it must be considered that the energy density of the plasma is higher than measured at RHIC. This increase in energy density leads to a larger energy loss of high-p_T partons with respect to those at both lower p_T (<3 GeV/c) and lower energy [26,27]. Moreover, it has been observed that baryons and strange mesons exhibit similar suppression as that of pions above 10 GeV/c. The measurement of another light meson, the η meson, provides additional information about mechanisms of particle production and energy loss, while the measurement of both mesons at higher p_T will give insight about the p_T dependence of the suppression in this region.

The suppression due to the QGP can also be studied with the η/π^0 ratio. In heavy-ion collisions, gluons are expected to experience larger energy loss in the medium than quarks, due to gluons having a larger vertex coupling factor. The energy reduction due to the presence of the medium (jet quenching effect) [28] may alter gluon and quark fragmentation differently with respect to what is observed in pp collisions. These differences between gluon and quark energy loss may introduce a modification in the suppression patterns observed for π^0 and η mesons, due to a larger gluon component in the η meson (note that the η meson, unlike π^0, has a two-gluon component) [29]. An intermediate p_T enhancement of the η/π^0 ratio in AA collisions relative to pp collisions would be an indication of the plasma-induced color dependence suppression [30–32]. The magnitude of this enhancement is sensitive to the initial values of the jet transport parameters and thus could be used to quantify the suppression.

In this paper, we present π^0 and η meson production measurements from the ALICE experiment in the p_T range $1 < p_T < 20$ GeV/c in Pb-Pb collisions at center-of-mass energy $\sqrt{s_{NN}} = 2.76$ TeV in two centrality classes, 0–10% and 20–50%. The results are measured at midrapidity using two complementary detection methods: the photon conversion method (PCM) and use of the Electromagnetic Calorimeter (EMCal) [33]. The π^0 results in the 0–10% centrality class have been combined with the previously published π^0 result measured with the Photon Spectrometer (PHOS) calorimeter [27]. The new π^0 measurement is updated with 10 times more statistics than the previous ALICE measurement [27] and extends the p_T reach from 12 GeV/c to 20 GeV/c. The η measurement is the first measurement of its kind at the LHC and has a wider p_T reach than what was previously measured at RHIC [34].

The paper is organized as follows: A brief description of the detectors used and of the data sample is given in Sec. II. The analysis procedure is described in Sec. III. The results and the comparison to other experimental measurements and to theoretical predictions are presented in Secs. IV and V, respectively.

II. DETECTOR DESCRIPTION AND DATA SAMPLE

The ALICE experiment and its performance are described in detail in Refs. [35,36]. The main detectors used for the reconstruction of π^0 and η mesons are located in the central barrel, operated inside a solenoidal magnetic field of 0.5 T directed along the beam axis.

The Inner Tracking System (ITS) is a high granularity and precision detector that measures the position of the primary collision vertex and the impact parameter of the tracks [37]. The ITS is composed of six cylindrical layers of silicon detectors positioned at radial distances from 4 to 43 cm. The two innermost layers of the ITS are Silicon Pixel Detectors (SPD) that cover the pseudorapidity regions $|\eta| < 2$ and $|\eta| < 1.4$. The next two layers are Silicon Drift Detectors (SDD) covering $|\eta| < 1$, while the two outer layers are Silicon Strip Detectors (SSD) covering $|\eta| < 0.9$.

The Time Projection Chamber (TPC) [38] is the main charged particle tracking and identification detector in the ALICE central barrel. It is a cylindrical drift detector filled with a Ne-CO_2 (90%-10%) gas mixture. This detector surrounds the ITS and is centered around the Interaction Point (IP) at a radial distance from 85 to 250 cm. The TPC has full azimuthal coverage and covers $|\eta| < 0.9$ for the full track length. Particles are identified through the measurement of their specific energy loss (dE/dx) in the detector with a 6.5% resolution in the 0–5% most central Pb-Pb [36,38]. The track's transverse-momentum resolution is $[\sigma(p_T)/p_T] = 0.8\%$ at 1 GeV/c and 1.7% at 10 GeV/c in central Pb-Pb collisions [36,39].

The EMCal [33] is a sampling calorimeter composed of 77 alternating layers of 1.4-mm lead and 1.7-mm polystyrene scintillators. The EMCal is a fairly high granularity detector. It has a cell area of $\Delta\eta \times \Delta\phi = 0.0143 \times 0.0143$ rad and an energy resolution of $\sigma_{E(\mathrm{GeV})}/E = 4.8\%/E \oplus 11.3/\sqrt{E} \oplus 1.7\%$ [40]. In year 2011, it covered $|\eta| < 0.7$ and $\Delta\varphi = 100^\circ$.

The main detectors used for triggering and characterization of the collision are the V0 [41] and the Zero Degree Calorimeters (ZDC) [42]. The V0 consists of two scintillator arrays located on opposite sides of the IP at 340 and 90 cm covering $2.8 < \eta < 5.1$ and $-3.7 < \eta < -1.7$, respectively. The ZDC detectors are located at a distance of 114 m on both sides of the IP and detect spectator nucleons.

The Pb-Pb data sample used for this analysis was collected in the 2011 LHC run. During that period, about 358 ion bunches circulated in each LHC beam, with collisions delivering a peak luminosity of 4.6×10^{-4} $\mu\mathrm{b}^{-1}\,\mathrm{s}^{-1}$, corresponding

to an average of about 10^{-3} hadronic interactions per bunch crossing. The minimum bias (MB) trigger was defined by the coincidence of signals in the two V0 arrays synchronized with a bunch crossing. An online selection based on the measured V0 amplitudes was employed to enhance central (0–10%) and semicentral (0–50%) events [36]. The ZDC and the V0 were also used for the rejection of pile-up and beam-gas interactions. The centrality class definition was based on the V0 amplitude distributions. The number of binary collisions ($N_{\rm coll}$) for a given value of the centrality was extracted with the help of a Glauber model [43] as detailed in Refs. [39,44]. Only events with a reconstructed primary vertex within $|z_{\rm vtx}| < 10$ cm of the nominal interaction vertex along the beam direction were accepted. The data are analyzed in two centrality classes: 0–10% and 20–50%, containing $1.9(1.6) \times 10^7$ and $1.3(1.1) \times 10^7$ events for PCM (EMCal), respectively. The minimum bias trigger cross section, $\sigma_{\rm MB}^{\rm PbPb} = [7.64 \pm 0.22({\rm syst.})]$ b [44], was determined using van der Meer scans [45]. The integrated luminosity, corresponding to the number of analyzed events normalized by $\sigma_{\rm MB}^{\rm PbPb}$ in each centrality percentile, is 20.1 $\mu{\rm b}^{-1}$ and 4.8 $\mu{\rm b}^{-1}$ for 0–10% and for 20–50%, respectively.

III. ANALYSIS METHODS

The π^0 and η mesons are reconstructed using the two-photon decay channel, $\pi^0 \to \gamma\gamma$ and $\eta \to \gamma\gamma$, with a branching ratio of $(98.823 \pm 0.034)\%$ and $(39.41 \pm 0.20)\%$ [1], respectively. With the photon conversion method, photons that convert in the detector material are measured by reconstructing the electron-positron pairs in the central rapidity detectors using a secondary vertex (V^0) finding algorithm [36]. This method produces a V^0 candidate sample on which the analysis quality selection criteria were applied, as done in Refs. [27,46]. Electrons, positrons, and photons are required to have $|\eta| < 0.9$. To ensure track quality, a minimum track momentum of 50 MeV/c and a fraction of TPC clusters over findable clusters (the number of geometrically possible clusters which can be assigned to a track) above 0.6 have been required. Moreover, a maximum conversion radius of 180 cm delimits the TPC fiducial volume for good track reconstruction, while a minimum of 5 cm rejects Dalitz decays of the type $\pi^0(\eta) \to e^+e^-\gamma$. The specific energy loss dE/dx should be within the interval $[-3\,\sigma_{dE/dx}, +5\sigma_{dE/dx}]$ from the expected electron Bethe-Bloch parametrization value, where σ is the standard deviation of the energy loss measurement. Pions are rejected by a selection of 3σ above the pion hypothesis in the range $0.4 < p < 2$ GeV/c and of 1σ for $p > 2$ GeV/c. The smaller rejection with respect to the previous Pb-Pb measurement translates into a larger efficiency at high p_T for the π^0 and η mesons. To further reject $\rm K_s^0$, Λ, and $\overline{\Lambda}$ from the V^0 candidates, a selection is applied on the components of the momenta relative to the V^0, using the asymmetry of the longitudinal momentum of the V^0 daughters $[\alpha_{V^0} = (p_L^{e^+} - p_L^{e^-})/(p_L^{e^+} + p_L^{e^-})]$, and on the transverse momentum of the electron with respect to the V^0 momentum ($q_T = p_e \times \sin\theta_{V^0,e}$). V^0 candidates are selected with a two-dimensional elliptic selection criterion of $(\alpha_{V^0}/\alpha_{V^0_{\rm max}})^2 + (q_{\rm T}/q_{T,{\rm max}})^2 < 1$, with $\alpha_{V^0_{\rm max}} = 0.95$ and $q_{T,{\rm max}} = 0.05$ GeV/c, in order to increase the purity while optimizing efficiency of the photon sample. As conversion electrons have a preferred decay orientation, a selection on $\psi_{\rm pair}$, the angle between the plane perpendicular to the magnetic field and the plane containing the electron and positron tracks, together with a cut on the photon χ^2 of the Kalman filter [47], further suppresses the contamination from non-photonic V^0 candidates. This cut, described in Ref. [48], is applied requiring $\chi^2_{\gamma,{\rm max}} = 20$ and $\psi_{\rm pair,max} = 0.1$. To improve the signal significance, a p_T-dependent cut on the energy asymmetry of the photons $|\alpha| < 0.65{\rm tanh}[1.8({\rm GeV}/c)^{-1} p_T]$ [where $\alpha = (E_{\gamma_1} - E_{\gamma_2})/(E_{\gamma_1} + E_{\gamma_2})$, p_T in GeV/c] is applied.

For the measurement with the EMCal, photons stemming from meson decays are measured directly. Photonlike hits in the detector are identified by energy deposits in the neighboring cells, which are grouped into clusters with a minimum size of two cells. A minimum energy per cell of 50 MeV is required. The cluster finding algorithm employs a seed energy of $E_{\rm seed} = 0.3$ GeV, which is slightly above the minimum ionizing particle threshold [36]. EMCal clusters that coincide within a window of $|\Delta\eta| < 0.025$ and $|\Delta\phi| < 0.05$ radians of a charged particle reconstructed in the TPC and projected to the EMCal surface are rejected. Each selected EMCal cluster is then required to have a total energy of at least 1.5 GeV to remove low-energy pairs consisting of predominantly combinatorial background and particle conversions in the material. A loose photonlike electromagnetic shower shape selection is applied to the clusters by looking at the eccentricity of the cluster via the weighted RMS of the shower energy along the major ellipse axis according to

$$\sigma^2_{\rm long} = \frac{s_{\eta\eta} + s_{\varphi\varphi}}{2} + \sqrt{\frac{(s_{\eta\eta} - s_{\varphi\varphi})^2}{4} + s^2_{\eta\varphi}}, \qquad (1)$$

where $s_{ij} = \langle ij\rangle - \langle i\rangle\langle j\rangle$ are the covariance matrix elements; i, j are cell indices in η or φ axes; and $\langle ij\rangle$ and $\langle i\rangle$, $\langle j\rangle$ are the second and the first moments of the cluster cells weighted with the cell energy logarithm [36,49–51]. The purpose of this loose shower shape selection $0.1 < \sigma^2_{\rm long} < 0.5$ (photons sit in a narrow peak centered at 0.25) is to remove noisy and very deformed or asymmetric cluster shapes which result from the merging of different particle showers produced nearby in the calorimeter.

For the PCM and EMCal analyses, the reconstructed two-photon invariant mass is measured in bins of p_T in the rapidity range $|y| < 0.85$ and $|y| < 0.7$, respectively. The p_T ranges in which the separate methods contribute are reported in Table I. In addition, a minimum photon pair opening angle of 5 mrad is used to reject background in the PCM analysis.

The background under the neutral meson signal contains combinatorial and correlated contributions. The combinatorial background is estimated with the event mixing method by mixing photons from different events but with similar photon multiplicity and topological (vertex location on the z axis and in the particular case of the PCM analysis the event plane angle) characteristics. The mixed event background is normalized to the reconstructed two-photon invariant mass in a region at higher mass with respect to the meson peak and

TABLE I. Transverse momentum ranges for the π^0 and η meson measurements. For the η meson in both centralities and for the π^0 in 20–50% centrality class the combination is between PCM and EMCal. For π^0 in the 0–10%, the final results are obtained combining PCM, EMCal, as well as previously published results using the PHOS detector [27].

	π^0			η	
	PCM	EMCal	PHOS	PCM	EMCal
0–10%	1–14 GeV/c	4–20 GeV/c	1–12 GeV/c	1–10 GeV/c	4–20 GeV/c
20–50%	1–14 GeV/c	4–20 GeV/c	–	1–10 GeV/c	4–20 GeV/c

subtracted. Additionally, various fitting functions for the total background are also used in order to obtain the number of mesons and to evaluate the corresponding systematic uncertainty (EMCal). The resulting invariant mass distributions are fit with either a Gaussian combined with a low-mass exponential tail [52] (PCM, to account for electron bremsstrahlung) on top of a linear function (PCM, to account for residual background) or with a Crystal Ball distribution [53] (EMCal) in order to obtain the position and width of the peak [36]. After subtracting the total background, the yields are extracted for each p_T bin by integrating the invariant mass distributions over a range that depends on the peak position and resolution. Figure 1 shows the invariant mass distribution for the π^0 and η mesons reconstructed with PCM and EMCal.

Corrections for geometrical acceptance, reconstruction efficiency, secondary π^0 from weak decays (the measured spectra of the relevant particles [54] are taken as input) and hadronic interactions and occupancy effects due to cluster overlaps (for EMCal) were estimated with a Monte Carlo simulation using HIJING [55] as the event generator. The simulated particles are propagated through the apparatus via GEANT3 [56], where a realistic detector response based on experimental conditions is applied in order to reproduce the performance of the ALICE detector during data taking. The simulated events are then analyzed with the same reconstruction and analysis selection criteria applied to the experimental data.

It was verified that the detector resolutions were well reproduced by the Monte Carlo simulations [36]. The mass peak positions and widths measured in the data for each centrality interval for the PCM (EMCal) analysis were reproduced within 0.5% (1.5%) or better, and the remaining discrepancies have been taken into account in the systematic uncertainties associated with the difference of the energy scale and position of the calorimeter between data and Monte Carlo.

In the PCM analysis, the pile-up contribution is estimated by analyzing the distance of closest approach distribution for the photon candidates, as done in Ref. [27]. The effect of pile-up in the EMCal analysis was verified to be negligible since the EMCal cell timing resolution is an order of magnitude better than the bunch crossing spacing of 200 ns used in the 2011 Pb-Pb run.

For both methods, the systematic uncertainties were studied by varying the selection criteria used in the two analyses and by studying the resulting variations of the fully corrected spectra in individual p_T bins. The largest contribution to the systematic uncertainties for the PCM analysis comes from the uncertainty in the material budget [36] and amounts to 9%. Other sources of systematic uncertainties include the yield extraction, track reconstruction, electron identification, and photon reconstruction (mainly for the η meson). The details of the PCM systematic uncertainties are listed in Table II.

The main source of systematic uncertainties for the neutral meson detection with the EMCal is associated with the particle identification criteria used to select photon pairs (PID).

The uncertainties due to the signal extraction in a given p_T interval are taken as the mean of the uncertainties obtained in all signal and background parametrizations. Variations on the values used for the meson identification selection criteria are also included and the RMS of these values is used as a systematic uncertainty.

The EMCal detector energy response was determined by analyzing test beam data [40]. Comparisons of the mass peak position and the energy-to-momentum ratios of electron tracks [57] in data and Monte Carlo simulations quantify the overall systematic uncertainty due to the Monte Carlo description of the energy response and position of the calorimeter. This uncertainty amounts to 8.6% of the invariant yield measurements.

Other sources of systematic uncertainties are the material budget, the p_T distribution of the simulations used for the extraction of efficiencies and the contribution from higher mass decays. The details of the EMCal systematic uncertainties are listed in Table II. When computing the η/π^0 ratio and the nuclear modification factor, fully and partially correlated errors, such as material budget and energy scale (EMCal only), are taken into account.

IV. RESULTS

A. Invariant yields of the π^0 and η meson

The invariant differential yields for π^0 and η mesons have been calculated employing

$$E\frac{d^3N}{dp^3} = \frac{1}{2\pi N_{\rm evt}}\frac{1}{B_{\rm Ratio}\,A\varepsilon}\frac{N_{\rm raw}}{p_T\Delta p_T\Delta y}, \qquad (2)$$

where $N_{\rm evt}$ is the number of events in the centrality class considered, $B_{\rm Ratio}$ is the branching ratio [1] for the process $\pi^0(\eta) \to \gamma\gamma$, $A\varepsilon$ are the corresponding acceptance and efficiency corrections, and $N_{\rm raw}$ corresponds to the reconstructed $\pi^0(\eta)$ raw yield within the rapidity range Δy and the transverse momentum bin Δp_T. The horizontal location of the data points is shifted towards lower p_T from the bin center by a few MeV and illustrates the p_T value where the differential

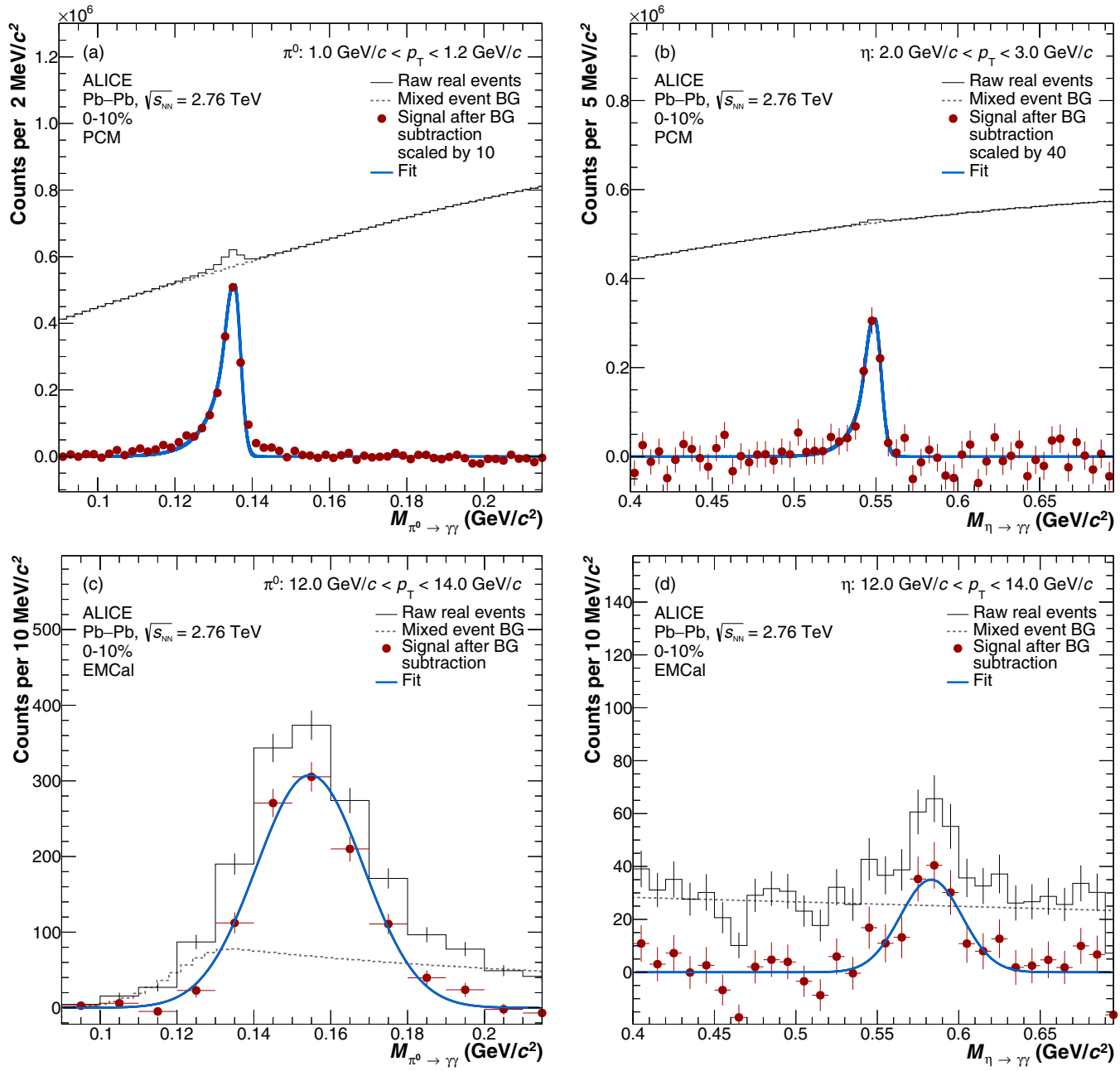

FIG. 1. Invariant mass distribution of reconstructed photon pairs $M_{\gamma\gamma}$ for the π^0 and η mesons measured with PCM [(a) and (b)] and EMCal [(c) and (d)] in the centrality class 0–10%. The black histograms show the signal before background subtraction while the red bullets show the signal after subtraction. The estimated background is indicated by the gray dashed lines. The blue lines are the fit to the invariant mass peak after the combinatorial and residual background subtraction (see text for description).

cross section is equal to the measured integral of the cross section over the corresponding bin [58]. For the η /π^0 ratio and R_{AA} the bin-shift correction is done in y coordinates. The p_T ranges in which the measurements were performed are reported in Table I. In the overlap region a weighted average of the two results (or three when applicable) is performed using the inverse of the quadratic sum of the uncertainties (statistical and systematic) that are uncorrelated between the methods as weights [59–61].

Figure 2 shows the invariant differential yields of (a) π^0 and (b) η meson measured in pp [51] and Pb-Pb collisions in the two centrality bins under study. The π^0 meson measurements are in agreement with the previously published ALICE π^0 spectra [27] and extend the transverse momentum reach from 12 to 20 GeV/c. For the η meson, the results presented here are the first measurement of its kind in heavy-ion collisions at the LHC and the first measurement of this meson to reach down to p_T of 1 GeV/c in a collider experiment [34,62].

Both meson spectra have been parametrized over the full p_T range by the function proposed in Refs. [63,64] that combines a Boltzmann factor at low p_T with a power law at

TABLE II. Summary of the systematic uncertainties in percentages for selected p_T regions for the PCM and EMCal analyses.

	PCM							
	0–10%				20–50%			
	π^0		η		π^0		η	
	1.1 GeV/c	5.5 GeV/c	2.5 GeV/c	5.0 GeV/c	1.1 GeV/c	5.5 GeV/c	2.5 GeV/c	5.0 GeV/c
Material budget	9.0	9.0	9.0	9.0	9.0	9.0	9.0	9.0
Track reconstruction	2.3	2.6	6.0	6.2	1.4	2.3	7.0	9.0
Yield extraction	1.5	2.1	6.4	7.0	2.5	2.8	10.0	11.0
e^+/e^- identification	1.7	2.5	6.0	6.1	1.4	2.4	5.5	9.3
Photon reconstruction	3.7	2.1	13.7	13.6	2.1	2.2	8.0	8.6
	EMCal							
	0–10%				20–50%			
	π^0		η		π^0		η	
	7.0 GeV/c	18.5 GeV/c	7.0 GeV/c	18.5 GeV/c	7.0 GeV/c	18.5 GeV/c	7.0 GeV/c	18.5 GeV/c
Signal extraction	2.9	5.1	4.2	5.5	7.5	5.8	6.0	7.1
Photon identification	9.5	8.0	4.6	6.0	7.5	4.5	14.1	5.0
Energy response	8.6	8.6	8.6	8.6	8.6	8.6	8.6	8.6
Material budget	5.0	5.0	5.0	5.0	5.0	5.0	5.0	5.0
Hijing simulation	8.6	10.0	8.6	10.0	2.0	5.3	2.0	5.3
Monte Carlo input	2.0	3.0	<1	1.5	<1	<1	<1	<1
Higher mass decays	4.0	2.0	–	–	3.2	2.0	–	–

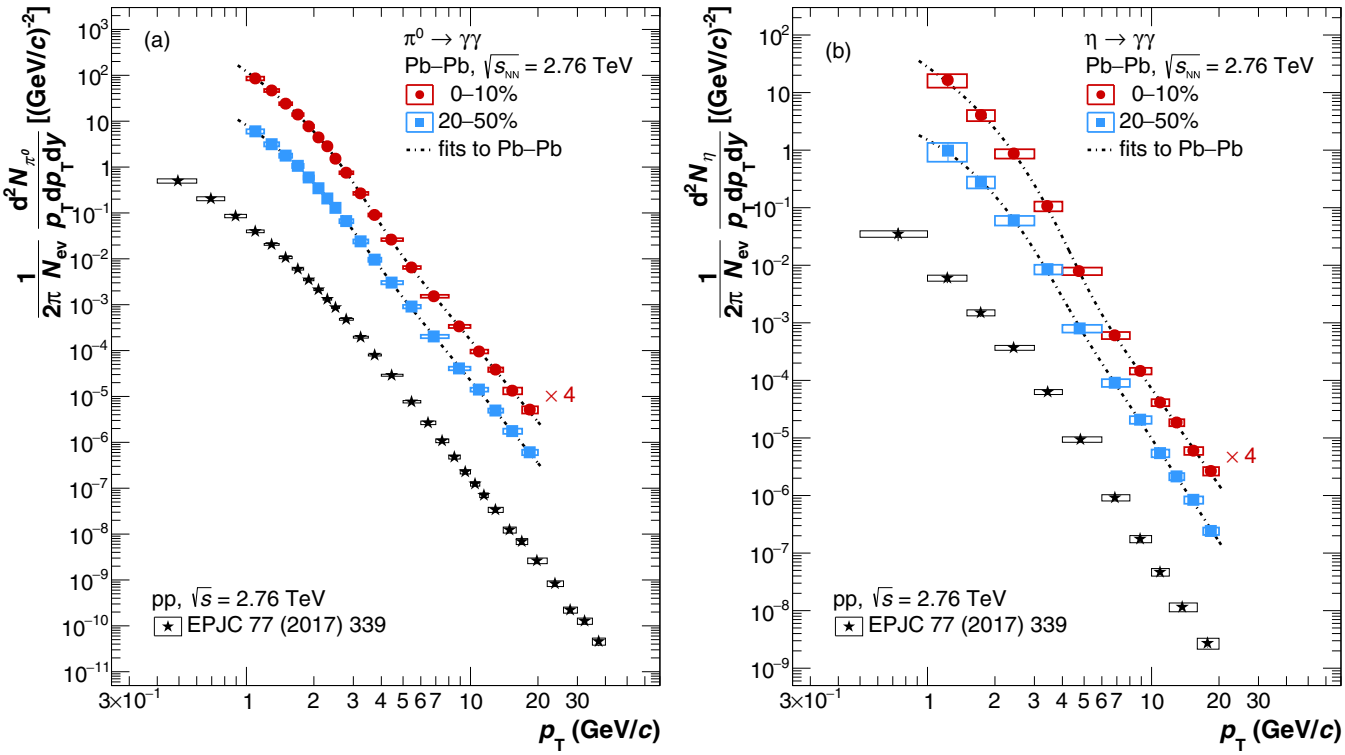

FIG. 2. Invariant yields of the (a) π^0 and (b) η meson in the centrality classes 0–10% (circles) and 20–50% (squares). The vertical error bars represent the statistical uncertainties while the boxes represent the systematic uncertainties. The Pb-Pb measurements are compared with the corresponding pp invariant cross sections (stars) measured at the same center-of-mass energy [27,51]. The dashed black lines correspond to the fits to the data with the two-component function. See Table III and corresponding text for details.

TABLE III. Parameters of the fits to the differential invariant yields of π^0 and η meson using the two-component function of Bylinkin and Rostovtsev [63,64]. The total uncertainties, i.e., quadratic sum of statistical and systematic uncertainties, are used for the fits.

	π^0		η	
	0–10%	20–50%	0–10%	20–50%
A_e (GeV/c)$^{-2}$	162 ± 20	30 ± 7	15 ± 6	4.2 ± 2.5
T_e (GeV/c)	0.37 ± 0.01	0.38 ± 0.02	0.44 ± 0.03	0.42 ± 0.06
A (GeV/c)$^{-2}$	840	80	100	2
T (GeV/c)	0.34 ± 0.01	0.50 ± 0.02	0.38 ± 0.03	0.76 ± 0.05
n	3.00 ± 0.05	3.00 ± 0.05	3.0 ± 0.1	3.0 ± 0.1
χ^2/ndf	0.18	0.20	0.22	0.14

high p_T,

$$E\frac{d^3N}{dp^3} = A_e \exp\frac{-\left(\sqrt{p_T^2+M^2}-M\right)}{T_e} + \frac{A}{\left(1+\frac{p_T^2}{T^2 n}\right)^n}, \quad (3)$$

where M is the meson mass (in GeV/c^2) and A_e, A, T_e, T, and n are free parameters of the fit. The parameters resulting from the fits to the meson invariant yields in both centrality classes are reported in Table III. All parameters are free except for the amplitude A. The values are chosen after a systematic study of the two separate components of the Bylinkin-Rostovtsev function and of the parameter limits variation.

B. Particle ratios

The η/π^0 ratio measured in the two centrality classes is shown in Fig. 3(a). In Fig. 3(b), the measurement in the 0–10% centrality class is compared to the same ratio measured in pp collisions at $\sqrt{s} = 2.76$ TeV [51], as well as to the $K^{\pm}/\pi^{\pm}$ ratio in the same centrality class and in the same collision system and energy [19], measured by ALICE. The $K^{\pm}/\pi^{\pm}$ ratio is of interest as the relative mass differences between these particles is similar to the one for the η and π^0 mesons. At $p_T < 2$ GeV/c, the η/π^0 and the $K^{\pm}/\pi^{\pm}$ ratios in Pb-Pb are in agreement within uncertainties. At $2 < p_T < 4$ GeV/c, due to the large uncertainties in the η/π^0 ratio in Pb-Pb, no conclusion can be made on the significance of the difference between the η/π^0 ratio in pp or the $K^{\pm}/\pi^{\pm}$ ratio in Pb-Pb. At $p_T > 4$ GeV/c, the value for all ratios is of similar magnitude. Moreover, a constant fit from 3 to 20 GeV/c gives a plateau value for the ratio of $0.457 \pm 0.013^{\text{stat}} \pm 0.018^{\text{syst}}$, in agreement with the value quoted in lower center-of-mass energy measurements [34].

C. The nuclear modification factor R_{AA}

The nuclear modification factor can be used to quantify particle production suppression in heavy-ion collisions with respect to pp collisions. It is defined as

$$R_{AA}(p_T) = \frac{d^2N/dy|_{AA}}{\langle T_{AA}\rangle \times d^2\sigma/dp_T dy|_{pp}}. \quad (4)$$

where the nuclear overlap function $\langle T_{AA}\rangle$ is related to the average number of inelastic collisions by $\langle T_{AA}\rangle = \langle N_{\text{coll}}\rangle/\sigma_{\text{inel}}^{pp}$

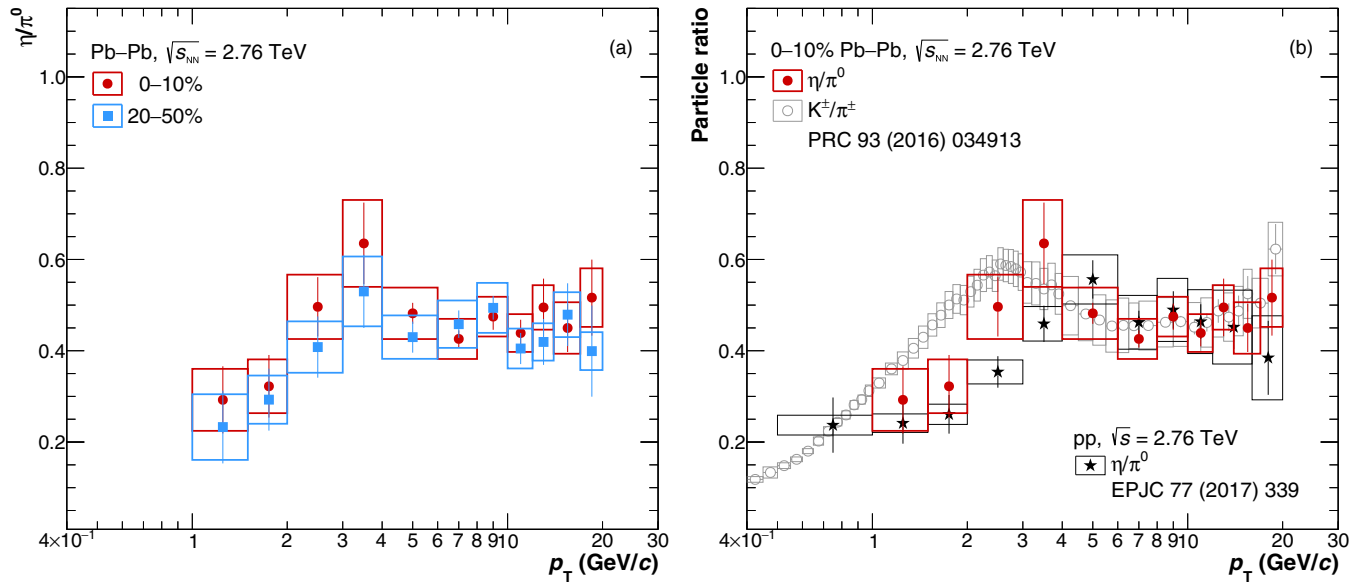

FIG. 3. (a) η/π^0 ratio in the two centrality classes measured, 0–10% (circles) and 20–50% (squares). (b) Comparison of the η/π^0 measurement in the 0–10% centrality class (full circles) to the corresponding ratio in pp collisions [51] (stars) and to the $K^{\pm}/\pi^{\pm}$ measurement in the same centrality class, system, and collision energy [19] (open circles).

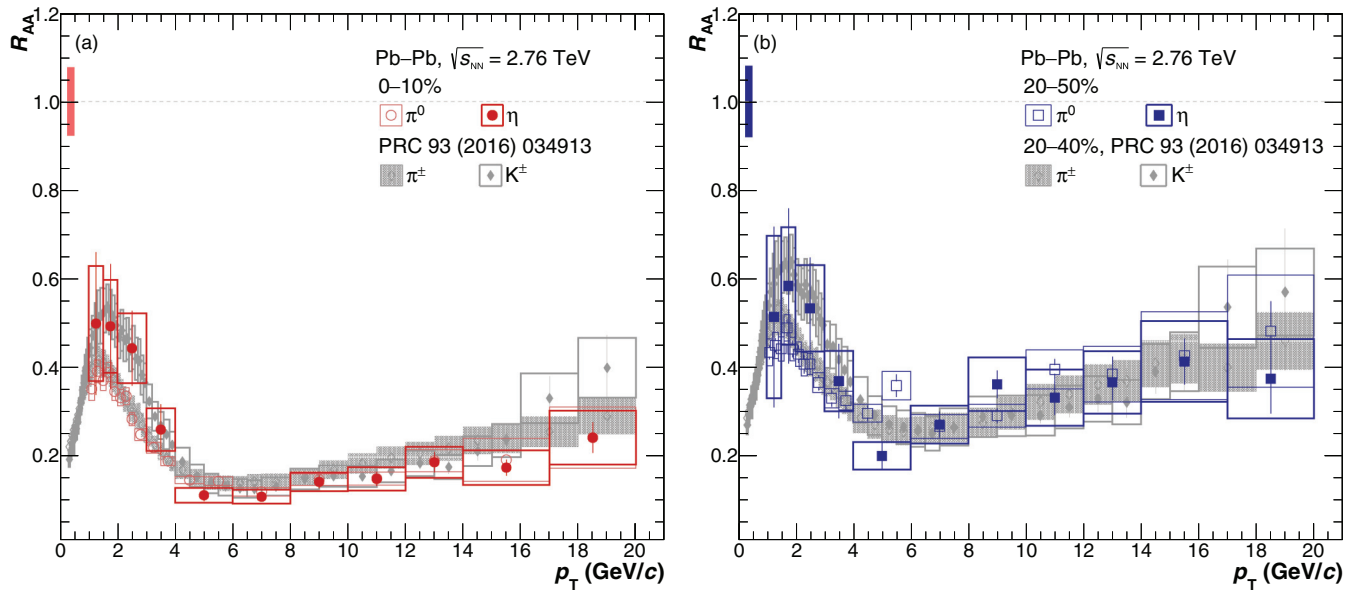

FIG. 4. Measured nuclear modification factor for the π^0(empty symbols) and η meson (full symbols) in the (a) 0–10% and (b) 20–50% centrality classes, compared to ALICE $\pi^\pm$ and $K^\pm$ [68,69] (open and full diamonds) in the same centrality classes. The boxes around unity represent quadratic sum of the uncertainty on $\langle T_{AA}\rangle$ and on the pp spectrum normalization uncertainty.

and $\sigma_{\text{inel}}^{pp}$ is the total inelastic cross section determined using van der Meer scans [65].

The mean number of collisions is 1501 ± 165 for the centrality class 0–10% and 349 ± 34 for the centrality class 20–50% [44]. The π^0 and η meson spectra measured in pp collisions at the same center-of-mass energy are obtained from Ref. [51].

The measured R_{AA} is presented in Fig. 4 for the π^0 and the η mesons. A p_T- and centrality-dependent suppression is clearly observed. For the most central collisions, the R_{AA} has a maximum around $p_T \approx 1.5$ GeV/c and a minimum for $p_T \approx 7$ GeV/c, after which it increases. The increase at high p_T could be due to the variation of the relative gluon and quark contributions to meson production as a function of p_T, with gluons being expected to suffer a stronger suppression than quarks due to a larger Casimir factor [66].

The suppression observed at high p_T is consistent with recent ATLAS results [67] and may indicate a larger quark than gluon relative contribution for high-p_T jet production in heavy-ion collisions at the LHC. A similar behavior is observed for semicentral events, though with a smaller suppression over the full transverse momentum range. The magnitude and pattern of the suppression is the same for the π^0 and η mesons for $p_T > 4$ GeV/c despite the difference in mass. At lower p_T, the present accuracy is not enough to determine if the suppression is different for the two mesons.

The R_{AA} values for both centrality classes are also compared to the ALICE charged kaon R_{AA} [68] measured at the same center-of-mass energy and collision system (Fig. 4) and is of interest given the similar masses of kaons and η mesons. This comparison indicates similar suppression patterns for η and $K^\pm$ across the whole p_T range and similar suppression between all particles for $p_T > 4$ GeV/c. This result is consistent with previous baryon and strange meson R_{AA} results [68,69], indicating that the energy loss in the medium is likely a purely partonic effect.

D. Comparisons to lower energy measurements

The nuclear modification factor in the 0–10% centrality class is compared to previous π^0 measurements reported by the WA98 [70] and PHENIX collaborations [25,71] [Fig. 5, (a)] for center-of-mass energies per binary collision $\sqrt{s_{NN}}$ ranging from 17.3 GeV (WA89) to 200 GeV (PHENIX).

Our results confirm a dependence of the suppression on the center-of-mass energy and indicate a larger suppression for increasing collision energy. At $p_T > 11$ GeV/c, the relative difference in suppression between the PHENIX and ALICE data is inconclusive due to the large uncertainties.

The η meson R_{AA} is compared to the corresponding PHENIX measurement [34] at $\sqrt{s_{NN}} = 200$ GeV [Fig. 5(b)]. Similarly to the π^0 case, the ALICE measurement shows a larger suppression compared to the PHENIX data in the region $5 < p_T < 14$ GeV/c.

V. COMPARISONS TO MODELS

The π^0 and η invariant p_T-differential yields are compared to predictions using a statistical hadronization model (SHM) [18,20] and the EPOS2 [72] event generator. Results from two versions of the SHM are presented here, an EQ and NEQ prediction. In the NEQ SHM, the mean particle multiplicities are described with the use of four thermodynamic parameters: temperature T, volume V, and two parameters to account for the nonequilibrium conditions—γ_s and γ_q. The EQ SHM can be treated as a particular case of the NEQ when $\gamma_s = \gamma_q = 1$. The parameters of the model are determined by fits to the measured charged pion and kaon spectra [20]. While only these two particles are considered in the fits, the

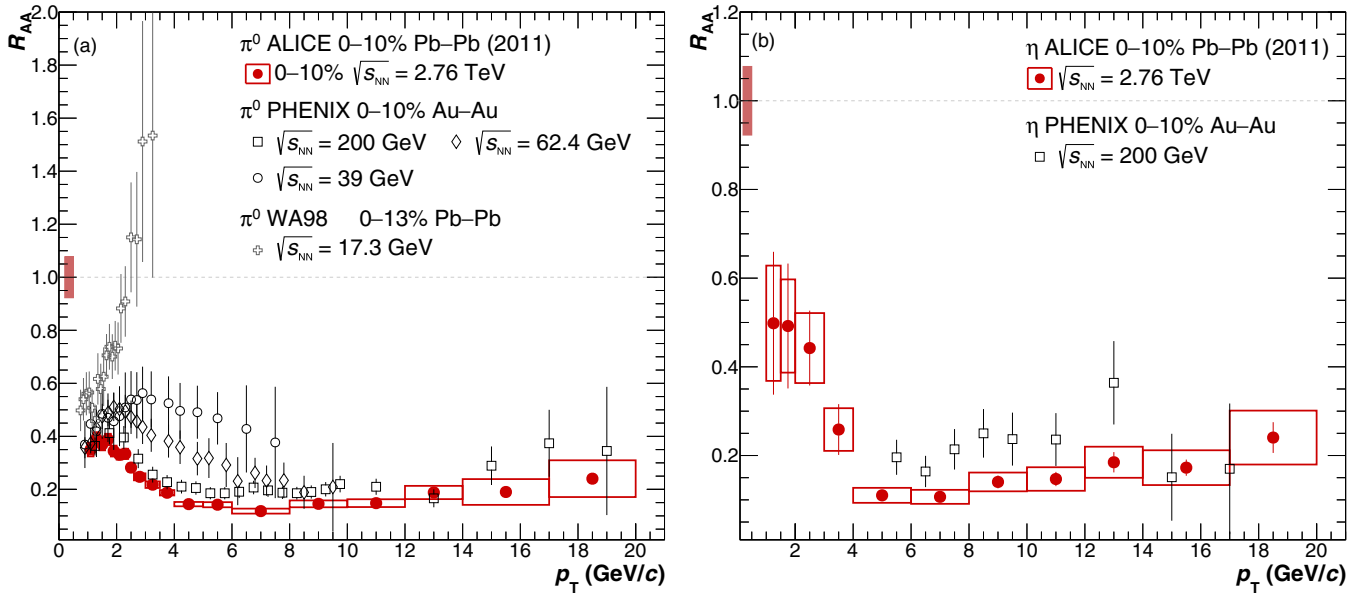

FIG. 5. R_{AA} of the (a) π^0 and (b) η meson compared to data from lower center-of-mass energy results [25,34,71].

resulting parameters are used to make predictions for other particles [73], e.g., the η meson, the ρ meson, and the proton. The EPOS generator addresses both low- and high-p_T phenomena, where the particle spectra include effects (low p_T) associated to hydrodynamic flow as discussed in Ref. [19]. At higher p_T, the focus is shifted towards energy loss of high-p_T strings where strings are the by-product of hard scatterings.

Figure 6(a) shows the comparison to models for the 0–10% and 20–50% centrality classes while Figs. 6(b)–6(e) shows the ratio of data and theory calculations to the fit of the π^0- and η-invariant yields.

The EQ and NEQ SHM predictions [bold lines in Figs. 6(b) and 6(c)] describe the shape of the π^0 measurement within the uncertainties for both centralities. For the η meson, in Figs. 6(d) and 6(e), the EQ model also describes the data within uncertainties. Conversely, the NEQ model predicts about half as many η mesons than actually measured in central collisions. The difference observed between the NEQ SHM and the data may point towards a different flow profile of the two mesons with a larger flow for the η than the π^0 [74]. Significant differences between the EQ and NEQ predictions are also observed for the ρ^0, $\Sigma(1385)$, $\Lambda(1520)$, and $\Xi(1530)$ [73,75].

The π^0 and η mesons are only partially described by EPOS [dashed lines in Figs. 6(b)–6(e)]. While the comparison is reasonably close to the data points for the π^0 measurement in 0–10% [Figs. 6(b)], the model only describes the low-p_T part of the [Fig. 6(c)] semicentral π^0 and [Figs. 6(d) and 6(e)] η measurements. No theoretical uncertainties for the EPOS calculations are available at the time of writing.

The η/π^0 ratio for the centrality class 0–10% is compared to the Next to Leading Order (NLO) pQCD calculation by Dai, Chen, Zhang, and Wang (DCZW) [30], to the ratio from the EQ and NEQ SHM [20] predictions, and to the EPOS [72] generator in Fig. 7. The DCZW model is based on a higher-twist approach to jet quenching [76] where parton fragmentation functions are modified as a consequence of the parton energy loss. A generalized QCD factorization of twist-4 processes is used to calculate the scattering. The effective parton fragmentation functions Albino, Kniehl, Kramer (AKK) [77] and Aidala, Ellinghaus, Seele, Stratmann (AESS) [78]) are then incorporated into a NLO pQCD framework to describe the particle production suppression. Data and the DCZW prediction are in agreement within uncertainties. The EQ SHM prediction describes the η/π^0 ratio, while in comparison to the NEQ SHM prediction the ratio is underestimated as shown in Figs. 6(d) and 6(e). The EPOS curves describe the ratio up to 4 GeV/c, as expected since the disagreement with the η meson measurement is larger at higher p_T.

The measurements of R_{AA} for both mesons are compared to four NLO pQCD-based models in Fig. 8: DCZW [30], Wicks, Horowitz, Djordjevic and Gyulassy (WHDG) [79–81], Djordevic *et al.* [82] (π^0 only), and Vitev *et al.* [83–86] (π^0 only). In the first three models, it is assumed that a fast-moving parton passing through hot partonic matter will lose its energy via induced radiation due to multiple parton scattering. The WHDG calculation models collisional and radiative energy loss processes in a Bjorken-expanding medium. It assumes that the color charge density of the medium is proportional to the number of participating nucleons obtained from a Glauber model. Hard parton-parton scatterings are then proportional to the number of binary nucleon-nucleon collisions. The Djordevic *et al.* model also includes effects due to the finite size of the QCD medium, the finite magnetic mass and the running of the coupling [82,87–89]. The model of Vitev *et al.* is an application of the soft-collinear effective theory with Glauber gluons ($SCET_G$) to study inclusive hadron suppression in nucleus-nucleus collisions. In this model, medium-evolved fragmentation functions are combined with all initial-state cold nuclear matter (CNM) effects (dynamical nuclear shadowing, Cronin effect and initial-state parton energy loss). The authors demonstrate that traditional

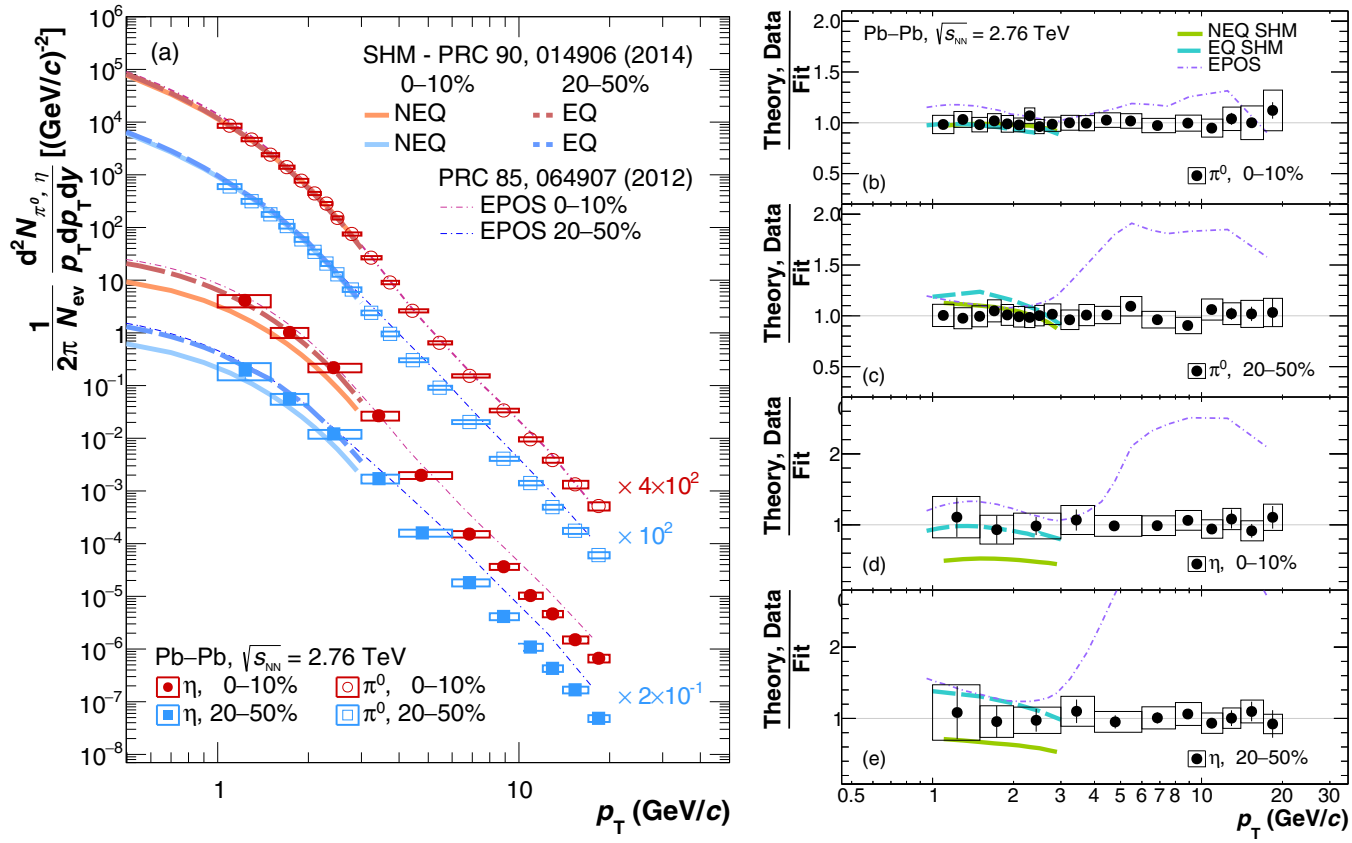

FIG. 6. (a) Comparison of the π^0(open symbols) and η (closed symbols) meson-invariant p_T-differential yields to EQ and NEQ SHM [20] and to EPOS [72] for the two centrality classes measured. [(b)–(e)] Ratio of data and theory calculations to the fit of the π^0- and η-invariant yields (see Fig. 2 and the left plot of this figure) in the two centrality classes measured. Black points show the data to fit ratio (vertical lines for statistical errors and boxes for systematic errors). The bold lines correspond to the ratio of the EQ and NEQ SHM predictions [20] to the data fit, while the thin dashed lines correspond to the same ratio for the EPOS predictions [72].

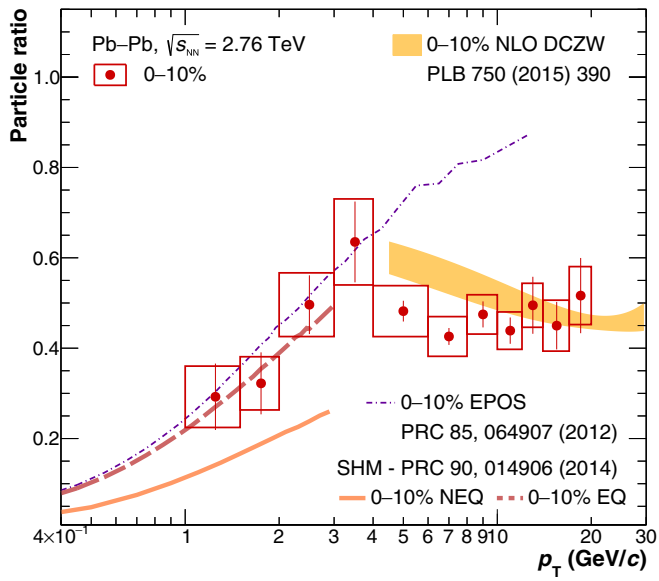

FIG. 7. Comparison of the η/π^0 ratio in the centrality class 0–10% (circles) to the NLO pQCD prediction by DCZW (solid band) [30] and to the EQ and NEQ SHM [20] and EPOS [72] predictions for the input yields (bold and thin dashed lines respectively).

parton energy loss calculations can be regarded as a special soft-gluon emission limit of the general QCD evolution framework.

In the most central event class, the π^0 meson R_{AA} is described for $p_T > 4$ GeV/c by the DCZW, Djordevic *et al.*, and Vitev *et al.* models and for $p_T > 6$ GeV/c by WHDG [Fig. 8(a)]. For the DCZW predictions, the η meson is described within uncertainties from $p_T > 8$ GeV/c; below this momentum, the DCZW model overstimates the R_{AA} result [Fig. 8(c)]. The latter may indicate that the relative quark and gluon contributions to the η meson production is overestimated at intermediate $p_T (4 < p_T < 8$ GeV/$c)$. On the other hand, the WHDG model predicts larger suppression than observed in the data for the η meson in the centrality class 0–10% and for both mesons in the centrality class 20–50%. The Djordevic *et al.* and Vitev *et al.* models describe the π^0 meson suppression in both centrality classes within uncertainties.

VI. SUMMARY

We have presented measurements of π^0 and η meson production at midrapidity in Pb-Pb collisions at $\sqrt{s_{NN}} = 2.76$ TeV measured with the ALICE detector. Independent and complementary techniques are used: pho-

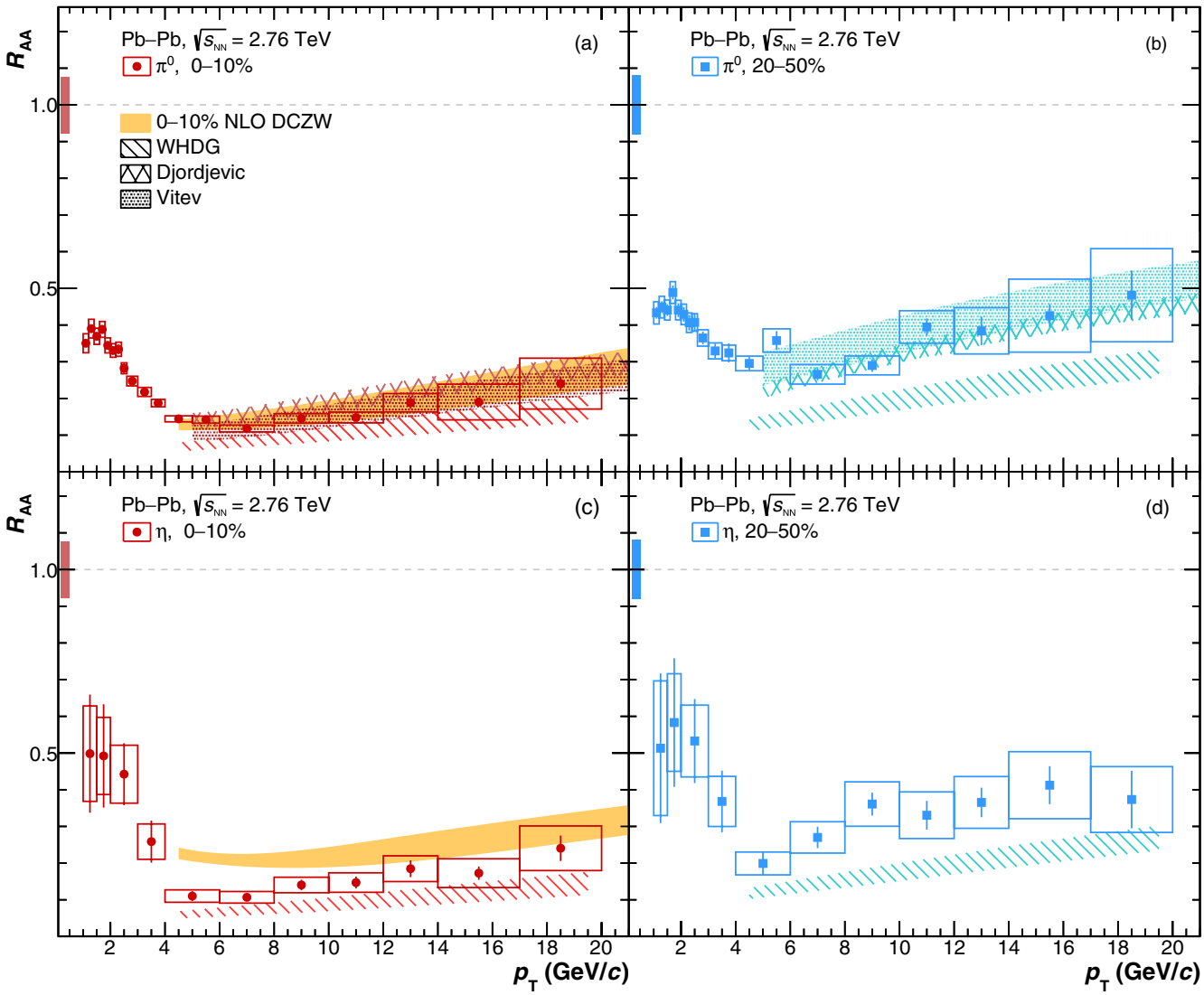

FIG. 8. R_{AA} of [(a) and (b)] π^0 and [(c) and (d)] η meson compared to NLO pQCD predictions by the DCZW (solid bands) [30], WHDG (dashed bands) [81], Djordevic *et al.* [82] (crossed bands, π^0 only), and Vitev *et al.* [83–86] (empty bands, π^0 only) models in the two centrality classes measured.

ton detection with electromagnetic calorimetry and photon reconstruction through conversions using the tracking system. The combination of these methods allowed measurements in a large transverse-momentum range, from 1 to 20 GeV/c.

The results represent the first measurement of η meson production in heavy-ion collisions at the LHC. The π^0 measurements are performed using data that correspond to a factor 10 increase in integrated luminosity with respect to the previous ALICE publication [27]. The higher statistics allowed for an improved measurement that probes the p_T region up to 20 GeV/c.

The η/π^0 ratio is compared to NLO pQCD calculations, corresponding ALICE measurements in pp collisions and to the $K^{\pm}/\pi^{\pm}$ ratio measured in Pb-Pb collisions at the same energy. For $p_T > 4$ GeV/c, these results indicate that the ratio in Pb-Pb is similar to the vacuum expectation, assuming this to be the pp measurement. The ratio is also consistent with predictions from pQCD-based calculations within experimental uncertainties. No effects beyond one σ related to the strange quark content, mass hierarchy between particles, or contributions from higher-mass resonance decays that may lead to discernible differences between η/π^0 and $K^{\pm}/\pi^{\pm}$ were observed.

The invariant yields of both mesons as well as the η/π^0 ratio are compared to predictions including a hydrodynamic approach focusing on low-p_T phenomena. These comparisons show different levels of agreement for η and π^0. EPOS slightly overestimates the production rates of the two mesons at low p_T but shows a much larger deviation above 3–4 GeV/c. Both the EQ and NEQ SHM predictions describe the measured π^0 production rates. The data favors the EQ model description which agrees with the η measurement. The NEQ model is disfavored by the data as it underestimates the results by a factor of two.

The RAA results show an increasing trend at high p_T which may be explained by a larger quark to gluon con-

tribution in the production of neutral mesons. The R_{AA} π^0 measurements, when compared to world data, confirm the center-of-mass energy dependence of the observed suppression when going from low (SPS) to higher (RHIC, ALICE) collision energies. Results of R_{AA} for η mesons are currently available only at two center-of-mass energies from the LHC and RHIC with sizable uncertainties. Due to the lack of precise world data, it is difficult to conclude on an energy dependence of the η suppression.

The R_{AA} results are additionally compared to NLO pQCD calculations. The WHDG model describes the suppression observed for the π^0 meson in the $0-10\%$ centrality class within theoretical and experimental uncertainties. For the η measurement, the model predicts a larger suppression than observed. In the 20–50% centrality class the predictions are in disagreement by several sigma with the ALICE data for both mesons. The DCZW model describes within uncertainties the π^0 measurement and the η meson above 8 GeV/c. Below this p_T, the model predicts less suppression than observed. The Djordevic *et al.* and Vitev *et al.* calculations describe well the π^0 production rates in both centrality classes. The disagreement observed between the η measurements and the models may point to a overestimation (DCZW) or underestimation (WHDG) of the gluon to quark contributions to the η meson production in heavy-ion collisions at LHC energies.

The presented results, when compared to models, highlight the lack of a full theoretical description of neutral meson production. The measurements presented in this paper will be essential to further constrain theoretical models and improve our understanding of the experimental results.

ACKNOWLEDGMENTS

We thank Viktor Begun, Wei Dai, Magdalena Djordevic, William Horowitz, Marco Stratmann, Ivan Vitev, and Klaus Werner for useful discussions and clarifications and for providing the predictions shown in this paper. The ALICE Collaboration thanks all its engineers and technicians for their invaluable contributions to the construction of the experiment and the CERN accelerator teams for the outstanding performance of the LHC complex. The ALICE Collaboration gratefully acknowledges the resources and support provided by all Grid centres and the Worldwide LHC Computing Grid (WLCG) collaboration. The ALICE Collaboration acknowledges the following funding agencies for their support in building and running the ALICE detector: A. I. Alikhanyan National Science Laboratory (Yerevan Physics Institute) Foundation (ANSL), State Committee of Science and World Federation of Scientists (WFS), Armenia; Austrian Academy of Sciences and Nationalstiftung für Forschung, Technologie und Entwicklung, Austria; Ministry of Communications and High Technologies, National Nuclear Research Center, Azerbaijan; Conselho Nacional de Desenvolvimento Científico e Tecnológico (CNPq), Universidade Federal do Rio Grande do Sul (UFRGS), Financiadora de Estudos e Projetos (Finep) and Fundação de Amparo à Pesquisa do Estado de São Paulo (FAPESP), Brazil; Ministry of Science & Technology of China (MSTC), National Natural Science Foundation of China (NSFC) and Ministry of Education of China (MOEC), China; Ministry of Science, Education and Sport and Croatian Science Foundation, Croatia; Ministry of Education, Youth and Sports of the Czech Republic, Czech Republic; The Danish Council for Independent Research | Natural Sciences, the Carlsberg Foundation and Danish National Research Foundation (DNRF), Denmark; Helsinki Institute of Physics (HIP), Finland; Commissariat à l'Energie Atomique (CEA) and Institut National de Physique Nucléaire et de Physique des Particules (IN2P3) and Centre National de la Recherche Scientifique (CNRS), France; Bundesministerium für Bildung, Wissenschaft, Forschung und Technologie (BMBF) and GSI Helmholtzzentrum für Schwerionenforschung GmbH, Germany; General Secretariat for Research and Technology, Ministry of Education, Research and Religions, Greece; National Research, Development and Innovation Office, Hungary; Department of Atomic Energy Government of India (DAE), Department of Science and Technology, Government of India (DST), University Grants Commission, Government of India (UGC) and Council of Scientific and Industrial Research (CSIR), India; Indonesian Institute of Science, Indonesia; Centro Fermi - Museo Storico della Fisica e Centro Studi e Ricerche Enrico Fermi and Istituto Nazionale di Fisica Nucleare (INFN), Italy; Institute for Innovative Science and Technology, Nagasaki Institute of Applied Science (IIST), Japan Society for the Promotion of Science (JSPS) KAKENHI and Japanese Ministry of Education, Culture, Sports, Science and Technology (MEXT), Japan; Consejo Nacional de Ciencia (CONACYT) y Tecnología, through Fondo de Cooperación Internacional en Ciencia y Tecnología (FONCICYT) and Dirección General de Asuntos del Personal Academico (DGAPA), Mexico; Nederlandse Organisatie voor Wetenschappelijk Onderzoek (NWO), Netherlands; The Research Council of Norway, Norway; Commission on Science and Technology for Sustainable Development in the South (COMSATS), Pakistan; Pontificia Universidad Católica del Perú, Peru; Ministry of Science and Higher Education and National Science Centre, Poland; Korea Institute of Science and Technology Information and National Research Foundation of Korea (NRF), Republic of Korea; Ministry of Education and Scientific Research, Institute of Atomic Physics and Romanian National Agency for Science, Technology and Innovation, Romania; Joint Institute for Nuclear Research (JINR), Ministry of Education and Science of the Russian Federation and National Research Centre Kurchatov Institute, Russia; Ministry of Education, Science, Research and Sport of the Slovak Republic, Slovakia; National Research Foundation of South Africa, South Africa; Swedish Research Council (VR) and Knut & Alice Wallenberg Foundation (KAW), Sweden; European Organization for Nuclear Research, Switzerland; National Science and Technology Development Agency (NSDTA), Suranaree University of Technology (SUT) and Office of the Higher Education Commission under NRU project of Thailand, Thailand; Turkish Atomic Energy Agency (TAEK), Turkey; National Academy of Sciences of Ukraine, Ukraine; Science and Technology Facilities Council (STFC), United Kingdom; National Science Foundation of the United States of America (NSF) and United States Department of Energy, Office of Nuclear Physics (DOE NP), United States of America.

[1] C. Patrignani *et al.* (Particle Data Group Collaboration), Review of particle physics, Chin. Phys. C **40**, 100001 (2016).

[2] H.-T. Ding, F. Karsch, and S. Mukherjee, Thermodynamics of strong-interaction matter from Lattice QCD, Int. J. Mod. Phys. E **24**, 1530007 (2015).

[3] P. Braun-Munzinger, V. Koch, T. Schaefer, and J. Stachel, Properties of hot and dense matter from relativistic heavy ion collisions, Phys. Rep. **621**, 76 (2016).

[4] D. Boyanovsky, H. J. de Vega, and D. J. Schwarz, Phase transitions in the early and the present universe, Annu. Rev. Nucl. Part. Sci. **56**, 441 (2006).

[5] Y. Aoki, G. Endrodi, Z. Fodor, S. D. Katz, and K. K. Szabo, The order of the quantum chromodynamics transition predicted by the standard model of particle physics, Nature **443**, 675 (2006).

[6] A. Bazavov *et al.* (HotQCD Collaboration), Equation of state in $(2+1)$-flavor QCD, Phys. Rev. D **90**, 094503 (2014).

[7] R. A. Soltz, C. DeTar, F. Karsch, S. Mukherjee, and P. Vranas, Lattice QCD thermodynamics with physical quark masses, Annu. Rev. Nucl. Part. Sci. **65**, 379 (2015).

[8] A. Bazavov, H. T. Ding, P. Hegde, F. Karsch, E. Laermann, S. Mukherjee, P. Petreczky, and C. Schmidt, Chiral phase structure of three flavor QCD at vanishing baryon number density, Phys. Rev. D **95**, 074505 (2017).

[9] A. Andronic, P. Braun-Munzinger, K. Redlich, and J. Stachel, Decoding the phase structure of QCD via particle production at high energy, arXiv:1710.09425 [nucl-th].

[10] J. E. Bernhard, J. S. Moreland, S. A. Bass, J. Liu, and U. Heinz, Applying Bayesian parameter estimation to relativistic heavy-ion collisions: simultaneous characterization of the initial state and quark-gluon plasma medium, Phys. Rev. C **94**, 024907 (2016).

[11] K. M. Burke *et al.* (JET Collaboration), Extracting the jet transport coefficient from jet quenching in high-energy heavy-ion collisions, Phys. Rev. C **90**, 014909 (2014).

[12] E. Wang and X.-N. Wang, Jet Tomography of Dense and Nuclear Matter, Phys. Rev. Lett. **89**, 162301 (2002).

[13] M. Wilde (ALICE Collaboration), Measurement of direct photons in pp and Pb-Pb collisions with ALICE, Nucl. Phys. A **904-905**, 573c (2013).

[14] B. B. Abelev *et al.* (ALICE Collaboration), Measurement of electrons from semileptonic heavy-flavor hadron decays in pp collisions at $\sqrt{s} = 2.76$ TeV, Phys. Rev. D **91**, 012001 (2015).

[15] J. Adam *et al.* (ALICE Collaboration), Direct photon production in Pb-Pb collisions at $\sqrt{s_{NN}} = 2.76$ TeV, Phys. Lett. B **754**, 235 (2016).

[16] A. Adare *et al.* (PHENIX Collaboration), Spectra and ratios of identified particles in Au-Au and dAu collisions at $\sqrt{s_{NN}} = 200$ GeV, Phys. Rev. C **88**, 024906 (2013).

[17] C. Adler *et al.* (STAR Collaboration), Multiplicity Distribution and Spectra of Negatively Charged Hadrons in Au-Au Collisions at $\sqrt{s_{NN}} = 130$ GeV, Phys. Rev. Lett. **87**, 112303 (2001).

[18] W. Broniowski and W. Florkowski, Explanation of the RHIC p_{T}-Spectra in a Thermal Model with Expansion, Phys. Rev. Lett. **87**, 272302 (2001).

[19] B. Abelev *et al.* (ALICE Collaboration), Centrality dependence of π, K, p production in Pb-Pb collisions at $\sqrt{s_{NN}} = 2.76$ TeV, Phys. Rev. C **88**, 044910 (2013).

[20] V. Begun, W. Florkowski, and M. Rybczynski, Explanation of hadron transverse-momentum spectra in heavy-ion collisions at $\sqrt{s_{NN}} = 2.76$ TeV within chemical nonequilibrium statistical hadronization model, Phys. Rev. C **90**, 014906 (2014).

[21] V. Begun and W. Florkowski, Bose-Einstein condensation of pions in heavy-ion collisions at the CERN Large Hadron Collider (LHC) energies, Phys. Rev. C **91**, 054909 (2015).

[22] H. Abuki, R. Anglani, R. Gatto, M. Pellicoro, and M. Ruggieri, The fate of pion condensation in quark matter: From the chiral to the real world, Phys. Rev. D **79**, 034032 (2009).

[23] A. B. Migdal, A. I. Chernoutsan, and I. N. Mishustin, Pion condensation and dynamics of neutron stars, Phys. Lett. B **83**, 158 (1979).

[24] A. Zee, *Quantum Field Theory in a Nutshell* (Princeton University Press, Princeton, NJ, 2003), p. 576.

[25] A. Adare *et al.* (PHENIX Collaboration), Evolution of π^0 Suppression in Au-Au Collisions from $\sqrt{s_{NN}} = 39$ to 200 GeV, Phys. Rev. Lett. **109**, 152301 (2012).

[26] K. Aamodt *et al.* (ALICE Collaboration), Suppression of charged particle production at large transverse momentum in central Pb-Pb collisions at $\sqrt{s_{NN}} = 2.76$ TeV, Phys. Lett. B **696** 30 (2011).

[27] B. B. Abelev *et al.* (ALICE Collaboration), Neutral pion production at midrapidity in pp and Pb-Pb collisions at $\sqrt{s_{NN}} = 2.76$ TeV, Eur. Phys. J. C **74**, 3108 (2014).

[28] N. Armesto *et al.* Comparison of jet quenching formalisms for a quark-gluon plasma brick, Phys. Rev. C **86**, 064904 (2012).

[29] P. Kroll and K. Passek-Kumericki, The two gluon components of the η and η' mesons to leading twist accuracy, Phys. Rev. D **67**, 054017 (2003).

[30] W. Dai, X.-F. Chen, B.-W. Zhang, and E. Wang, η meson production of high-energy nuclear collisions at NLO, Phys. Lett. B **750**, 390 (2015).

[31] M. Gyulassy and M. Plumer, Jet quenching in dense matter, Phys. Lett. B **243**, 432 (1990).

[32] R. Baier, Y. L. Dokshitzer, A. H. Mueller, S. Peigne, and D. Schiff, Radiative energy loss and p_{T} broadening of high-energy partons in nuclei, Nucl. Phys. B **484**, 265 (1997).

[33] P. Cortese *et al.* ALICE electromagnetic calorimeter technical design report, Tech. Rep. CERN-LHCC-2008-014, CERN-ALICE-TDR-014, ALICE Collaboration, 2008.

[34] S. S. Adler *et al.* (PHENIX Collaboration), Common Suppression Pattern of η and π^0 Mesons at High Transverse Momentum in Au-Au Collisions at $\sqrt{s_{NN}} = 200$ GeV, Phys. Rev. Lett. **96**, 202301 (2006).

[35] K. Aamodt *et al.* (ALICE Collaboration), The ALICE experiment at the CERN LHC, JINST **3**, S08002 (2008).

[36] B. B. Abelev *et al.* (ALICE Collaboration), Performance of the ALICE Experiment at the CERN LHC, Int. J. Mod. Phys. A **29**, 1430044 (2014).

[37] K. Aamodt *et al.* (ALICE Collaboration), Alignment of the ALICE Inner Tracking System with cosmic-ray tracks, JINST **5**, P03003 (2010), arXiv:1001.0502 [physics.ins-det].

[38] J. Alme *et al.* (The ALICE TPC, a large 3-dimensional tracking device with fast readout for ultra-high multiplicity events, Nucl. Instrum. Methods A **622**, 316 (2010).

[39] B. Abelev *et al.* (ALICE Collaboration), Centrality dependence of charged particle production at large transverse momentum in Pb-Pb collisions at $\sqrt{s_{NN}} = 2.76$ TeV, Phys. Lett. B **720**, 52 (2013).

[40] J. Allen *et al.* (ALICE EMCal Collaboration), Performance of prototypes for the ALICE electromagnetic calorimeter, Nucl. Instrum. Methods A **615**, 6 (2010).

[41] E. Abbas *et al.* (ALICE Collaboration), Performance of the ALICE VZERO system, JINST **8**, P10016 (2013).

[42] B. Abelev *et al.* (ALICE Collaboration), Measurement of the Cross Section for Electromagnetic Dissociation with Neutron Emission in Pb-Pb Collisions at $\sqrt{s_{NN}} = 2.76$ TeV, Phys. Rev. Lett. **109**, 252302 (2012).

[43] M. L. Miller, K. Reygers, S. J. Sanders, and P. Steinberg, Glauber modeling in high energy nuclear collisions, Annu. Rev. Nucl. Part. Sci. **57**, 205 (2007).

[44] B. Abelev *et al.* (ALICE Collaboration), Centrality determination of Pb-Pb collisions at $\sqrt{s_{NN}} = 2.76$ TeV with ALICE, Phys. Rev. C **88**, 044909 (2013).

[45] S. van der Meer, Calibration of the effective beam height in the ISR, Tech. Rep. CERN-ISR-PO-68-31. ISR-PO-68-31, CERN, Geneva, 1968. https://cds.cern.ch/record/296752

[46] B. Abelev *et al.* (ALICE Collaboration), Neutral pion and η meson production in proton-proton collisions at $\sqrt{s} = 0.9$ TeV and $\sqrt{s} = 7$ TeV, Phys. Lett. B **717**, 162 (2012).

[47] I. Kisel, I. Kulakov, and M. Zyzak, Standalone first level event selection package for the CBM experiment, IEEE Trans. Nucl. Sci. **60**, 3703 (2013).

[48] S. Acharya *et al.* (ALICE Collaboration), π^0 and η meson production in proton-proton collisions at $\sqrt{s = 8}$ TeV, Eur. Phys. J. C **78**, 263 (2018).

[49] H. Grassmann and H. G. Moser, Shower shape analysis and longitudinal sampled electromagnetic calorimeter, Nucl. Instrum. Methods A **237**, 486 (1985).

[50] P. Cortese *et al.* (ALICE Collaboration), ALICE: Physics performance report, volume II, J. Phys. G **32**, 1295 (2006).

[51] S. Acharya *et al.* (ALICE Collaboration), Production of and η mesons up to high transverse momentum in pp collisions at 2.76 TeV, Eur. Phys. J. C **77**, 339 (2017).

[52] T. Matulewicz *et al.* (Response of BaF_2 detectors to photons of 3–50 MeV energy, Nucl. Instrum. Methods A **289**, 194 (1990).

[53] J. Gaiser *et al.* (Charmonium spectroscopy from inclusive ψ' and J/ψ radiative decays, Phys. Rev. D **34**, 711 (1986).

[54] B. B. Abelev *et al.* (ALICE Collaboration), K^0_S and Λ Production in Pb-Pb Collisions at $\sqrt{s_{NN}} = 2.76$ TeV, Phys. Rev. Lett. **111**, 222301 (2013).

[55] M. Gyulassy and X.-N. Wang, HIJING 1.0: A Monte Carlo program for parton and particle production in high-energy hadronic and nuclear collisions, Comput. Phys. Commun. **83**, 307 (1994).

[56] R. Brun *et al. CERN Program Library Long Write-up W5013* (1994). [http://wwwasd.web.cern.ch/wwwasd/geant/]

[57] J. Adam *et al.* (ALICE Collaboration), Measurement of the production of high-p_T electrons from heavy-flavour hadron decays in Pb-Pb collisions at $\sqrt{s_{NN}} = 2.76$ TeV, Phys. Lett. B **771**, 467 (2017).

[58] G. D. Lafferty and T. R. Wyatt, Where to stick your data points: The treatment of measurements within wide bins, Nucl. Instrum. Methods A **355**, 541 (1995).

[59] L. Lyons, D. Gibaut, and P. Clifford, How to combine correlated estimates of a single physical quantity, Nucl. Instrum. Methods A **270**, 110 (1988).

[60] A. Valassi, Combining correlated measurements of several different physical quantities, Nucl. Instrum. Methods A **500**, 391 (2003).

[61] A. Valassi and R. Chierici, Information and treatment of unknown correlations in the combination of measurements using the BLUE method, Eur. Phys. J. C **74**, 2717 (2014).

[62] S. S. Adler *et al.* (PHENIX Collaboration), High transverse momentum η meson production in pp, dAu and Au-Au collisions at $\sqrt{s_{NN}} = 200$ GeV, Phys. Rev. C **75**, 024909 (2007).

[63] A. A. Bylinkin and A. A. Rostovtsev, Parametrization of the shape of hadron-production spectra in high-energy particle interactions, Phys. Atom. Nucl. **75**, 999 (2012); Physics of Atomic Nuclei Yad. Fiz. **75**, 1060 (2012).

[64] A. Bylinkin, N. S. Chernyavskaya, and A. A. Rostovtsev, Predictions on the transverse momentum spectra for charged particle production at LHC-energies from a two component model, Eur. Phys. J. C **75**, 166 (2015).

[65] B. Abelev *et al.* (ALICE Collaboration), Measurement of inelastic, single- and double-diffraction cross sections in proton–proton collisions at the LHC with ALICE, Eur. Phys. J. C **73**, 2456 (2013).

[66] S. Sarkar, H. Satz, and B. Sinha, *The Physics of the Quark-Gluon Plasma: Introductory Lectures*, Vol. 785 of Lecture Notes in Physics (Springer, Heidelberg, 2010).

[67] M. Aaboud *et al.* (ATLAS Collaboration), Measurement of jet fragmentation in Pb-Pb and pp collisions at $\sqrt{s_{\rm NN}} = 2.76$ TeV with the ATLAS detector at the LHC, Eur. Phys. J. C **77**, 379 (2017).

[68] J. Adam *et al.* (ALICE Collaboration), Centrality dependence of the nuclear modification factor of charged pions, kaons, and protons in Pb-Pb collisions at $\sqrt{s_{\rm NN}} = 2.76$ TeV, Phys. Rev. C **93**, 034913 (2016).

[69] B. B. Abelev *et al.* (ALICE Collaboration), Production of charged pions, kaons and protons at large transverse momenta in pp and Pb-Pb collisions at $\sqrt{s_{NN}} = 2.76$ TeV, Phys. Lett. B **736**, 196 (2014).

[70] M. M. Aggarwal *et al.* (WA98 Collaboration), Suppression of High-p_T Neutral Pions in Central Pb-Pb Collisions at $\sqrt{s_{NN}} =$ 17.3 GeV, Phys. Rev. Lett. **100**, 242301 (2008).

[71] A. Adare *et al.* (PHENIX Collaboration), Suppression Pattern of Neutral Pions at High Transverse Momentum in Au-Au Collisions at $\sqrt{s_{NN}} = 200$ GeV and Constraints on Medium Transport Coefficients, Phys. Rev. Lett. **101**, 232301 (2008).

[72] K. Werner, I. Karpenko, M. Bleicher, T. Pierog, and S. Porteboeuf-Houssais, Jets, bulk matter, and their interaction in heavy-ion collisions at several TeV, Phys. Rev. C **85**, 064907 (2012).

[73] V. Begun, Resonances in a sudden chemical freeze-out model, EPJ Web Conf. **171**, 15002 (2018).

[74] F. Retiere and M. A. Lisa, Observable implications of geometrical and dynamical aspects of freeze-out in heavy ion collisions, Phys. Rev. C **70**, 044907 (2004).

[75] V. Begun, W. Florkowski, and M. Rybczynski, Transverse-momentum spectra of strange particles produced in Pb-Pb collisions at $\sqrt{s_{NN}} = 2.76$ TeV in the chemical nonequilibrium model, Phys. Rev. C **90**, 054912 (2014).

[76] X.-f. Guo and X.-N. Wang, Multiple Scattering, Parton Energy Loss and Modified Fragmentation Functions in Deeply Inelastic Scattering, Phys. Rev. Lett. **85**, 3591 (2000).

[77] S. Albino, B. A. Kniehl, and G. Kramer, Fragmentation functions for light charged hadrons with complete quark flavor separation, Nucl. Phys. B **725**, 181 (2005).

[78] C. A. Aidala, F. Ellinghaus, R. Sassot, J. P. Seele, and M. Stratmann, Global analysis of fragmentation functions for η mesons, Phys. Rev. D **83**, 034002 (2011).

[79] S. Wicks, W. Horowitz, M. Djordjevic, and M. Gyulassy, Elastic, inelastic, and path length fluctuations in jet tomography, Nucl. Phys. A **784**, 426 (2007).
[80] W. A. Horowitz and M. Gyulassy, The surprising transparency of the sQGP at LHC, Nucl. Phys. A **872**, 265 (2011).
[81] W. A. Horowitz, LHC predictions from an extended theory with elastic, inelastic, and path length fluctuating energy loss, Int. J. Mod. Phys. E **16**, 2193 (2007).
[82] M. Djordjevic and M. Djordjevic, LHC jet suppression of light and heavy flavor observables, Phys. Lett. B **734**, 286 (2014).
[83] I. Vitev, Testing the mechanism of QGP-induced energy loss, Phys. Lett. B **639**, 38 (2006).
[84] Z.-B. Kang, R. Lashof-Regas, G. Ovanesyan, P. Saad, and I. Vitev, Jet Quenching Phenomenology from Soft-Collinear Effective Theory with Glauber Gluons, Phys. Rev. Lett. **114**, 092002 (2015).
[85] Y.-T. Chien, A. Emerman, Z.-B. Kang, G. Ovanesyan, and I. Vitev, Jet quenching from QCD evolution, Phys. Rev. D **93**, 074030 (2016).
[86] C. W. Bauer, B. O. Lange, and G. Ovanesyan, On Glauber modes in soft-collinear effective theory, J. High Energy Phys. 07 (2011) 077.
[87] M. Djordjevic, Collisional energy loss in a finite size QCD matter, Phys. Rev. C **74**, 064907 (2006).
[88] M. Djordjevic and U. W. Heinz, Radiative Energy Loss in a Finite Dynamical QCD Medium, Phys. Rev. Lett. **101**, 022302 (2008).
[89] M. Djordjevic and M. Djordjevic, Generalization of radiative jet energy loss to non-zero magnetic mass, Phys. Lett. B **709**, 229 (2012).

S. Acharya,[138] F. T.-. Acosta,[22] D. Adamová,[94] J. Adolfsson,[81] M. M. Aggarwal,[98] G. Aglieri Rinella,[36] M. Agnello,[33] N. Agrawal,[48] Z. Ahammed,[138] S. U. Ahn,[77] S. Aiola,[143] A. Akindinov,[64] M. Al-Turany,[104] S. N. Alam,[138] D. S. D. Albuquerque,[119] D. Aleksandrov,[88] B. Alessandro,[58] R. Alfaro Molina,[72] Y. Ali,[16] A. Alici,[29,11,53] A. Alkin,[3] J. Alme,[24] T. Alt,[69] L. Altenkamper,[24] I. Altsybeev,[137] C. Andrei,[47] D. Andreou,[36] H. A. Andrews,[108] A. Andronic,[104] M. Angeletti,[36] V. Anguelov,[102] C. Anson,[17] T. Antičić,[105] F. Antinori,[56] P. Antonioli,[53] N. Apadula,[80] L. Aphecetche,[111] H. Appelshäuser,[69] S. Arcelli,[29] R. Arnaldi,[58] O. W. Arnold,[103,114] I. C. Arsene,[23] M. Arslandok,[102] B. Audurier,[111] A. Augustinus,[36] R. Averbeck,[104] M. D. Azmi,[18] A. Badalà,[55] Y. W. Baek,[60,76] S. Bagnasco,[58] R. Bailhache,[69] R. Bala,[99] A. Baldisseri,[134] M. Ball,[43] R. C. Baral,[66,86] A. M. Barbano,[28] R. Barbera,[30] F. Barile,[35] L. Barioglio,[28] G. G. Barnaföldi,[142] L. S. Barnby,[93] V. Barret,[131] P. Bartalini,[7] K. Barth,[36] E. Bartsch,[69] N. Bastid,[131] S. Basu,[140] G. Batigne,[111] B. Batyunya,[75] P. C. Batzing,[23] J. L. Bazo Alba,[109] I. G. Bearden,[89] H. Beck,[102] C. Bedda,[63] N. K. Behera,[60] I. Belikov,[133] F. Bellini,[36,29] H. Bello Martinez,[2] R. Bellwied,[123] L. G. E. Beltran,[117] V. Belyaev,[92] G. Bencedi,[142] S. Beole,[28] A. Bercuci,[47] Y. Berdnikov,[96] D. Berenyi,[142] R. A. Bertens,[127] D. Berzano,[58,36] L. Betev,[36] P. P. Bhaduri,[138] A. Bhasin,[99] I. R. Bhat,[99] B. Bhattacharjee,[42] J. Bhom,[115] A. Bianchi,[28] L. Bianchi,[123] N. Bianchi,[51] C. Bianchin,[140] J. Bielčík,[38] J. Bielčíková,[94] A. Bilandzic,[114,103] G. Biro,[142] R. Biswas,[4] S. Biswas,[4] J. T. Blair,[116] D. Blau,[88] C. Blume,[69] G. Boca,[135] F. Bock,[36] A. Bogdanov,[92] L. Boldizsár,[142] M. Bombara,[39] G. Bonomi,[136] M. Bonora,[36] H. Borel,[134] A. Borissov,[102,20] M. Borri,[125] E. Botta,[28] C. Bourjau,[89] L. Bratrud,[69] P. Braun-Munzinger,[104] M. Bregant,[118] T. A. Broker,[69] M. Broz,[38] E. J. Brucken,[44] E. Bruna,[58] G. E. Bruno,[36,35] D. Budnikov,[106] H. Buesching,[69] S. Bufalino,[33] P. Buhler,[110] P. Buncic,[36] O. Busch,[130] Z. Buthelezi,[73] J. B. Butt,[16] J. T. Buxton,[19] J. Cabala,[113] D. Caffarri,[36,90] H. Caines,[143] A. Caliva,[63,104] E. Calvo Villar,[109] R. S. Camacho,[2] P. Camerini,[27] A. A. Capon,[110] F. Carena,[36] W. Carena,[36] F. Carnesecchi,[11,29] J. Castillo Castellanos,[134] A. J. Castro,[127] E. A. R. Casula,[54] C. Ceballos Sanchez,[9] S. Chandra,[138] B. Chang,[124] W. Chang,[7] S. Chapeland,[36] M. Chartier,[125] S. Chattopadhyay,[138] S. Chattopadhyay,[107] A. Chauvin,[114,103] C. Cheshkov,[132] B. Cheynis,[132] V. Chibante Barroso,[36] D. D. Chinellato,[119] S. Cho,[60] P. Chochula,[36] M. Chojnacki,[89] S. Choudhury,[138] T. Chowdhury,[131] P. Christakoglou,[90] C. H. Christensen,[89] P. Christiansen,[81] T. Chujo,[130] S. U. Chung,[20] C. Cicalo,[54] L. Cifarelli,[11,29] F. Cindolo,[53] J. Cleymans,[122] F. Colamaria,[52,35] D. Colella,[36,52,65] A. Collu,[80] M. Colocci,[29] M. Concas,[58,a] G. Conesa Balbastre,[79] Z. Conesa del Valle,[61] J. G. Contreras,[38] T. M. Cormier,[95] Y. Corrales Morales,[58] I. Cortés Maldonado,[2] P. Cortese,[34] M. R. Cosentino,[120] F. Costa,[36] S. Costanza,[135] J. Crkovská,[61] P. Crochet,[131] E. Cuautle,[70] L. Cunqueiro,[95,141] T. Dahms,[103,114] A. Dainese,[56] M. C. Danisch,[102] A. Danu,[68] D. Das,[107] I. Das,[107] S. Das,[4] A. Dash,[86] S. Dash,[48] S. De,[49] A. De Caro,[32] G. de Cataldo,[52] C. de Conti,[118] J. de Cuveland,[40] A. De Falco,[26] D. De Gruttola,[32,11] N. De Marco,[58] S. De Pasquale,[32] R. D. De Souza,[119] H. F. Degenhardt,[118] A. Deisting,[104,102] A. Deloff,[85] S. Delsanto,[28] C. Deplano,[90] P. Dhankher,[48] D. Di Bari,[35] A. Di Mauro,[36] P. Di Nezza,[51] B. Di Ruzza,[56] R. A. Diaz,[9] T. Dietel,[122] P. Dillenseger,[69] Y. Ding,[7] R. Divià,[36] Ø. Djuvsland,[24] A. Dobrin,[36] D. Domenicis Gimenez,[118] B. Dönigus,[69] O. Dordic,[23] L. V. R. Doremalen,[63] A. K. Dubey,[138] A. Dubla,[104] L. Ducroux,[132] S. Dudi,[98] A. K. Duggal,[98] M. Dukhishyam,[86] P. Dupieux,[131] R. J. Ehlers,[143] D. Elia,[52] E. Endress,[109] H. Engel,[74] E. Epple,[143] B. Erazmus,[111] F. Erhardt,[97] B. Espagnon,[61] G. Eulisse,[36] J. Eum,[20] D. Evans,[108] S. Evdokimov,[91] L. Fabbietti,[103,114] M. Faggin,[31] J. Faivre,[79] A. Fantoni,[51] M. Fasel,[95] L. Feldkamp,[141] A. Feliciello,[58] G. Feofilov,[137] A. Fernández Téllez,[2] A. Ferretti,[28] A. Festanti,[31,36] V. J. G. Feuillard,[134,131] J. Figiel,[115] M. A. S. Figueredo,[118] S. Filchagin,[106] D. Finogeev,[62] F. M. Fionda,[24,26] M. Floris,[36] S. Foertsch,[73] P. Foka,[104] S. Fokin,[88] E. Fragiacomo,[59] A. Francescon,[36] A. Francisco,[111] U. Frankenfeld,[104] G. G. Fronze,[28] U. Fuchs,[36] C. Furget,[79] A. Furs,[62] M. Fusco Girard,[32] J. J. Gaardhøje,[89] M. Gagliardi,[28] A. M. Gago,[109] K. Gajdosova,[89] M. Gallio,[28] C. D. Galvan,[117] P. Ganoti,[84] C. Garabatos,[104] E. Garcia-Solis,[12] K. Garg,[30] C. Gargiulo,[36] P. Gasik,[114,103] E. F. Gauger,[116] M. B. Gay Ducati,[71] M. Germain,[111] J. Ghosh,[107] P. Ghosh,[138] S. K. Ghosh,[4]

P. Gianotti,[51] P. Giubellino,[58,104,36] P. Giubilato,[31] E. Gladysz-Dziadus,[115] P. Glässel,[102] D. M. Goméz Coral,[72] A. Gomez Ramirez,[74] A. S. Gonzalez,[36] P. González-Zamora,[2] S. Gorbunov,[40] L. Görlich,[115] S. Gotovac,[126] V. Grabski,[72] L. K. Graczykowski,[139] K. L. Graham,[108] L. Greiner,[80] A. Grelli,[63] C. Grigoras,[36] V. Grigoriev,[92] A. Grigoryan,[1] S. Grigoryan,[75] J. M. Gronefeld,[104] F. Grosa,[33] J. F. Grosse-Oetringhaus,[36] R. Grosso,[104] F. Guber,[62] R. Guernane,[79] B. Guerzoni,[29] M. Guittiere,[111] K. Gulbrandsen,[89] T. Gunji,[129] A. Gupta,[99] R. Gupta,[99] I. B. Guzman,[2] R. Haake,[36] M. K. Habib,[104] C. Hadjidakis,[61] H. Hamagaki,[82] G. Hamar,[142] J. C. Hamon,[133] M. R. Haque,[63] J. W. Harris,[143] A. Harton,[12] H. Hassan,[79] D. Hatzifotiadou,[53,11] S. Hayashi,[129] S. T. Heckel,[69] E. Hellbär,[69] H. Helstrup,[37] A. Herghelegiu,[47] E. G. Hernandez,[2] G. Herrera Corral,[10] F. Herrmann,[141] B. A. Hess,[101] K. F. Hetland,[37] H. Hillemanns,[36] C. Hills,[125] B. Hippolyte,[133] B. Hohlweger,[103] D. Horak,[38] S. Hornung,[104] R. Hosokawa,[130,79] P. Hristov,[36] C. Hughes,[127] P. Huhn,[69] T. J. Humanic,[19] H. Hushnud,[107] N. Hussain,[42] T. Hussain,[18] D. Hutter,[40] D. S. Hwang,[21] J. P. Iddon,[125] S. A. Iga Buitron,[70] R. Ilkaev,[106] M. Inaba,[130] M. Ippolitov,[92,88] M. S. Islam,[107] M. Ivanov,[104] V. Ivanov,[96] V. Izucheev,[91] B. Jacak,[80] N. Jacazio,[29] P. M. Jacobs,[80] M. B. Jadhav,[48] S. Jadlovska,[113] J. Jadlovsky,[113] S. Jaelani,[63] C. Jahnke,[118,114] M. J. Jakubowska,[139] M. A. Janik,[139] P. H. S. Y. Jayarathna,[123] C. Jena,[86] M. Jercic,[97] R. T. Jimenez Bustamante,[104] P. G. Jones,[108] A. Jusko,[108] P. Kalinak,[65] A. Kalweit,[36] J. H. Kang,[144] V. Kaplin,[92] S. Kar,[138] A. Karasu Uysal,[78] O. Karavichev,[62] T. Karavicheva,[62] L. Karayan,[104,102] P. Karczmarczyk,[36] E. Karpechev,[62] U. Kebschull,[74] R. Keidel,[46] D. L. D. Keijdener,[63] M. Keil,[36] B. Ketzer,[43] Z. Khabanova,[90] S. Khan,[18] S. A. Khan,[138] A. Khanzadeev,[96] Y. Kharlov,[91] A. Khatun,[18] A. Khuntia,[49] M. M. Kielbowicz,[115] B. Kileng,[37] B. Kim,[130] D. Kim,[144] D. J. Kim,[124] E. J. Kim,[14] H. Kim,[144] J. S. Kim,[41] J. Kim,[102] M. Kim,[60] S. Kim,[21] T. Kim,[144] S. Kirsch,[40] I. Kisel,[40] S. Kiselev,[64] A. Kisiel,[139] G. Kiss,[142] J. L. Klay,[6] C. Klein,[69] J. Klein,[36] C. Klein-Bösing,[141] S. Klewin,[102] A. Kluge,[36] M. L. Knichel,[102,36] A. G. Knospe,[123] C. Kobdaj,[112] M. Kofarago,[142] M. K. Köhler,[102] T. Kollegger,[104] V. Kondratiev,[137] N. Kondratyeva,[92] E. Kondratyuk,[91] A. Konevskikh,[62] M. Konyushikhin,[140] M. Kopcik,[113] C. Kouzinopoulos,[36] O. Kovalenko,[85] V. Kovalenko,[137] M. Kowalski,[115] I. Králik,[65] A. Kravčáková,[39] L. Kreis,[104] M. Krivda,[108,65] F. Krizek,[94] M. Krüger,[69] E. Kryshen,[96] M. Krzewicki,[40] A. M. Kubera,[19] V. Kučera,[94] C. Kuhn,[133] P. G. Kuijer,[90] J. Kumar,[48] L. Kumar,[98] S. Kumar,[48] S. Kundu,[86] P. Kurashvili,[85] A. Kurepin,[62] A. B. Kurepin,[62] A. Kuryakin,[106] S. Kushpil,[94] M. J. Kweon,[60] Y. Kwon,[144] S. L. La Pointe,[40] P. La Rocca,[30] C. Lagana Fernandes,[118] Y. S. Lai,[80] I. Lakomov,[36] R. Langoy,[121] K. Lapidus,[143] C. Lara,[74] A. Lardeux,[23] P. Larionov,[51] A. Lattuca,[28] E. Laudi,[36] R. Lavicka,[38] R. Lea,[27] L. Leardini,[102] S. Lee,[144] F. Lehas,[90] S. Lehner,[110] J. Lehrbach,[40] R. C. Lemmon,[93] E. Leogrande,[63] I. León Monzón,[117] P. Lévai,[142] X. Li,[13] X. L. Li,[7] J. Lien,[121] R. Lietava,[108] B. Lim,[20] S. Lindal,[23] V. Lindenstruth,[40] S. W. Lindsay,[125] C. Lippmann,[104] M. A. Lisa,[19] V. Litichevskyi,[44] A. Liu,[80] H. M. Ljunggren,[81] W. J. Llope,[140] D. F. Lodato,[63] P. I. Loenne,[24] V. Loginov,[92] C. Loizides,[95,80] P. Loncar,[126] X. Lopez,[131] E. López Torres,[9] A. Lowe,[142] P. Luettig,[69] J. R. Luhder,[141] M. Lunardon,[31] G. Luparello,[59,27] M. Lupi,[36] A. Maevskaya,[62] M. Mager,[36] S. M. Mahmood,[23] A. Maire,[133] R. D. Majka,[143] M. Malaev,[96] L. Malinina,[75,b] D. Mal'Kevich,[64] P. Malzacher,[104] A. Mamonov,[106] V. Manko,[88] F. Manso,[131] V. Manzari,[52] Y. Mao,[7] M. Marchisone,[73,128,132] J. Mareš,[67] G. V. Margagliotti,[27] A. Margotti,[53] J. Margutti,[63] A. Marín,[104] C. Markert,[116] M. Marquard,[69] N. A. Martin,[104] P. Martinengo,[36] J. A. L. Martinez,[74] M. I. Martínez,[2] G. Martínez García,[111] M. Martinez Pedreira,[36] S. Masciocchi,[104] M. Masera,[28] A. Masoni,[54] L. Massacrier,[61] E. Masson,[111] A. Mastroserio,[52] A. M. Mathis,[103,114] P. F. T. Matuoka,[118] A. Matyja,[127] C. Mayer,[115] J. Mazer,[127] M. Mazzilli,[35] M. A. Mazzoni,[57] F. Meddi,[25] Y. Melikyan,[92] A. Menchaca-Rocha,[72] E. Meninno,[32] J. Mercado Pérez,[102] M. Meres,[15] S. Mhlanga,[122] Y. Miake,[130] L. Micheletti,[28] M. M. Mieskolainen,[44] D. L. Mihaylov,[103] K. Mikhaylov,[64,75] A. Mischke,[63] D. Miśkowiec,[104] J. Mitra,[138] C. M. Mitu,[68] N. Mohammadi,[36,63] A. P. Mohanty,[63] B. Mohanty,[86] M. Mohisin Khan,[18,c] D. A. Moreira De Godoy,[141] L. A. P. Moreno,[2] S. Moretto,[31] A. Morreale,[111] A. Morsch,[36] V. Muccifora,[51] E. Mudnic,[126] D. Mühlheim,[141] S. Muhuri,[138] M. Mukherjee,[4] J. D. Mulligan,[143] M. G. Munhoz,[118] K. Münning,[43] M. I. A. Munoz,[80] R. H. Munzer,[69] H. Murakami,[129] S. Murray,[73] L. Musa,[36] J. Musinsky,[65] C. J. Myers,[123] J. W. Myrcha,[139] B. Naik,[48] R. Nair,[85] B. K. Nandi,[48] R. Nania,[11,53] E. Nappi,[52] A. Narayan,[48] M. U. Naru,[16] H. Natal da Luz,[118] C. Nattrass,[127] S. R. Navarro,[2] K. Nayak,[86] R. Nayak,[48] T. K. Nayak,[138] S. Nazarenko,[106] R. A. Negrao De Oliveira,[36,69] L. Nellen,[70] S. V. Nesbo,[37] G. Neskovic,[40] F. Ng,[123] M. Nicassio,[104] M. Niculescu,[68] J. Niedziela,[139,36] B. S. Nielsen,[89] S. Nikolaev,[88] S. Nikulin,[88] V. Nikulin,[96] A. Nobuhiro,[45] F. Noferini,[11,53] P. Nomokonov,[75] G. Nooren,[63] J. C. C. Noris,[2] J. Norman,[79,125] A. Nyanin,[88] J. Nystrand,[24] H. Oeschler,[20,102,d] H. Oh,[144] A. Ohlson,[102] L. Olah,[142] J. Oleniacz,[139] A. C. Oliveira Da Silva,[118] M. H. Oliver,[143] J. Onderwaater,[104] C. Oppedisano,[58] R. Orava,[44] M. Oravec,[113] A. Ortiz Velasquez,[70] A. Oskarsson,[81] J. Otwinowski,[115] K. Oyama,[82] Y. Pachmayer,[102] V. Pacik,[89] D. Pagano,[136] G. Paić,[70] P. Palni,[7] J. Pan,[140] A. K. Pandey,[48] S. Panebianco,[134] V. Papikyan,[1] P. Pareek,[49] J. Park,[60] S. Parmar,[98] A. Passfeld,[141] S. P. Pathak,[123] R. N. Patra,[138] B. Paul,[58] H. Pei,[7] T. Peitzmann,[63] X. Peng,[7] L. G. Pereira,[71] H. Pereira Da Costa,[134] D. Peresunko,[92,88] E. Perez Lezama,[69] V. Peskov,[69] Y. Pestov,[5] V. Petráček,[38] M. Petrovici,[47] C. Petta,[30] R. P. Pezzi,[71] S. Piano,[59] M. Pikna,[15] P. Pillot,[111] L. O. D. L. Pimentel,[89] O. Pinazza,[53,36] L. Pinsky,[123] S. Pisano,[51] D. B. Piyarathna,[123] M. Płoskoń,[80] M. Planinic,[97] F. Pliquett,[69] J. Pluta,[139] S. Pochybova,[142] P. L. M. Podesta-Lerma,[117] M. G. Poghosyan,[95] B. Polichtchouk,[91] N. Poljak,[97] W. Poonsawat,[112] A. Pop,[47] H. Poppenborg,[141] S. Porteboeuf-Houssais,[131] V. Pozdniakov,[75] S. K. Prasad,[4] R. Preghenella,[53] F. Prino,[58] C. A. Pruneau,[140] I. Pshenichnov,[62] M. Puccio,[28] V. Punin,[106] J. Putschke,[140] S. Raha,[4] S. Rajput,[99] J. Rak,[124] A. Rakotozafindrabe,[134] L. Ramello,[34] F. Rami,[133] D. B. Rana,[123] R. Raniwala,[100] S. Raniwala,[100] S. S. Räsänen,[44] B. T. Rascanu,[69] D. Rathee,[98] V. Ratza,[43] I. Ravasenga,[33] K. F. Read,[127,95] K. Redlich,[85,e] A. Rehman,[24] P. Reichelt,[69] F. Reidt,[36] X. Ren,[7] R. Renfordt,[69] A. Reshetin,[62] K. Reygers,[102] V. Riabov,[96] T. Richert,[63,81] M. Richter,[23] P. Riedler,[36] W. Riegler,[36] F. Riggi,[30] C. Ristea,[68] M. Rodríguez Cahuantzi,[2]

K. Røed,[23] R. Rogalev,[91] E. Rogochaya,[75] D. Rohr,[36,40] D. Röhrich,[24] P. S. Rokita,[139] F. Ronchetti,[51] E. D. Rosas,[70] K. Roslon,[139] P. Rosnet,[131] A. Rossi,[31,56] A. Rotondi,[135] F. Roukoutakis,[84] C. Roy,[133] P. Roy,[107] O. V. Rueda,[70] R. Rui,[27] B. Rumyantsev,[75] A. Rustamov,[87] E. Ryabinkin,[88] Y. Ryabov,[96] A. Rybicki,[115] S. Saarinen,[44] S. Sadhu,[138] S. Sadovsky,[91] K. Šafařík,[36] S. K. Saha,[138] B. Sahoo,[48] P. Sahoo,[49] R. Sahoo,[49] S. Sahoo,[66] P. K. Sahu,[66] J. Saini,[138] S. Sakai,[130] M. A. Saleh,[140] J. Salzwedel,[19] S. Sambyal,[99] V. Samsonov,[96,92] A. Sandoval,[72] A. Sarkar,[73] D. Sarkar,[138] N. Sarkar,[138] P. Sarma,[42] M. H. P. Sas,[63] E. Scapparone,[53] F. Scarlassara,[31] B. Schaefer,[95] H. S. Scheid,[69] C. Schiaua,[47] R. Schicker,[102] C. Schmidt,[104] H. R. Schmidt,[101] M. O. Schmidt,[102] M. Schmidt,[101] N. V. Schmidt,[69,95] J. Schukraft,[36] Y. Schutz,[36,133] K. Schwarz,[104] K. Schweda,[104] G. Scioli,[29] E. Scomparin,[58] M. Šefčík,[39] J. E. Seger,[17] Y. Sekiguchi,[129] D. Sekihata,[45] I. Selyuzhenkov,[92,104] K. Senosi,[73] S. Senyukov,[133] E. Serradilla,[72] P. Sett,[48] A. Sevcenco,[68] A. Shabanov,[62] A. Shabetai,[111] R. Shahoyan,[36] W. Shaikh,[107] A. Shangaraev,[91] A. Sharma,[98] A. Sharma,[99] N. Sharma,[98] A. I. Sheikh,[138] K. Shigaki,[45] M. Shimomura,[83] S. Shirinkin,[64] Q. Shou,[7] K. Shtejer,[9,28] Y. Sibiriak,[88] S. Siddhanta,[54] K. M. Sielewicz,[36] T. Siemiarczuk,[85] S. Silaeva,[88] D. Silvermyr,[81] G. Simatovic,[90,97] G. Simonetti,[36,103] R. Singaraju,[138] R. Singh,[86] V. Singhal,[138] T. Sinha,[107] B. Sitar,[15] M. Sitta,[34] T. B. Skaali,[23] M. Slupecki,[124] N. Smirnov,[143] R. J. M. Snellings,[63] T. W. Snellman,[124] J. Song,[20] F. Soramel,[31] S. Sorensen,[127] F. Sozzi,[104] I. Sputowska,[115] J. Stachel,[102] I. Stan,[68] P. Stankus,[95] E. Stenlund,[81] D. Stocco,[111] M. M. Storetvedt,[37] P. Strmen,[15] A. A. P. Suaide,[118] T. Sugitate,[45] C. Suire,[61] M. Suleymanov,[16] M. Suljic,[27] R. Sultanov,[64] M. Šumbera,[94] S. Sumowidagdo,[50] K. Suzuki,[110] S. Swain,[66] A. Szabo,[15] I. Szarka,[15] U. Tabassam,[16] J. Takahashi,[119] G. J. Tambave,[24] N. Tanaka,[130] M. Tarhini,[111,61] M. Tariq,[18] M. G. Tarzila,[47] A. Tauro,[36] G. Tejeda Muñoz,[2] A. Telesca,[36] K. Terasaki,[129] C. Terrevoli,[31] B. Teyssier,[132] D. Thakur,[49] S. Thakur,[138] D. Thomas,[116] F. Thoresen,[89] R. Tieulent,[132] A. Tikhonov,[62] A. R. Timmins,[123] A. Toia,[69] M. Toppi,[51] S. R. Torres,[117] S. Tripathy,[49] S. Trogolo,[28] G. Trombetta,[35] L. Tropp,[39] V. Trubnikov,[3] W. H. Trzaska,[124] T. P. Trzcinski,[139] B. A. Trzeciak,[63] T. Tsuji,[129] A. Tumkin,[106] R. Turrisi,[56] T. S. Tveter,[23] K. Ullaland,[24] E. N. Umaka,[123] A. Uras,[132] G. L. Usai,[26] A. Utrobicic,[97] M. Vala,[113] J. Van Der Maarel,[63] J. W. Van Hoorne,[36] M. van Leeuwen,[63] T. Vanat,[94] P. Vande Vyvre,[36] D. Varga,[142] A. Vargas,[2] M. Vargyas,[124] R. Varma,[48] M. Vasileiou,[84] A. Vasiliev,[88] A. Vauthier,[79] O. Vázquez Doce,[103,114] V. Vechernin,[137] A. M. Veen,[63] A. Velure,[24] E. Vercellin,[28] S. Vergara Limón,[2] L. Vermunt,[63] R. Vernet,[8] R. Vértesi,[142] L. Vickovic,[126] J. Viinikainen,[124] Z. Vilakazi,[128] O. Villalobos Baillie,[108] A. Villatoro Tello,[2] A. Vinogradov,[88] L. Vinogradov,[137] T. Virgili,[32] V. Vislavicius,[81] A. Vodopyanov,[75] M. A. Völkl,[101] K. Voloshin,[64] S. A. Voloshin,[140] G. Volpe,[35] B. von Haller,[36] I. Vorobyev,[103,114] D. Voscek,[113] D. Vranic,[36,104] J. Vrláková,[39] B. Wagner,[24] H. Wang,[63] M. Wang,[7] Y. Watanabe,[129,130] M. Weber,[110] S. G. Weber,[104] A. Wegrzynek,[36] D. F. Weiser,[102] S. C. Wenzel,[36] J. P. Wessels,[141] U. Westerhoff,[141] A. M. Whitehead,[122] J. Wiechula,[69] J. Wikne,[23] G. Wilk,[85] J. Wilkinson,[53] G. A. Willems,[36,141] M. C. S. Williams,[53] E. Willsher,[108] B. Windelband,[102] W. E. Witt,[127] R. Xu,[7] S. Yalcin,[78] K. Yamakawa,[45] P. Yang,[7] S. Yano,[45] Z. Yin,[7] H. Yokoyama,[79,130] I.-K. Yoo,[20] J. H. Yoon,[60] E. Yun,[20] V. Yurchenko,[3] V. Zaccolo,[58] A. Zaman,[16] C. Zampolli,[36] H. J. C. Zanoli,[118] N. Zardoshti,[108] A. Zarochentsev,[137] P. Závada,[67] N. Zaviyalov,[106] H. Zbroszczyk,[139] M. Zhalov,[96] H. Zhang,[24,7] X. Zhang,[7] Y. Zhang,[7] C. Zhang,[63] Z. Zhang,[7,131] C. Zhao,[23] N. Zhigareva,[64] D. Zhou,[7] Y. Zhou,[89] Z. Zhou,[24] H. Zhu,[7,24] J. Zhu,[7] Y. Zhu,[7] A. Zichichi,[29,11] M. B. Zimmermann,[36] G. Zinovjev,[3] J. Zmeskal,[110] and S. Zou[7]

(ALICE Collaboration)

[1]*A. I. Alikhanyan National Science Laboratory (Yerevan Physics Institute) Foundation, Yerevan, Armenia*
[2]*Benemérita Universidad Autónoma de Puebla, Puebla, Mexico*
[3]*Bogolyubov Institute for Theoretical Physics, National Academy of Sciences of Ukraine, Kiev, Ukraine*
[4]*Bose Institute, Department of Physics and Centre for Astroparticle Physics and Space Science (CAPSS), Kolkata, India*
[5]*Budker Institute for Nuclear Physics, Novosibirsk, Russia*
[6]*California Polytechnic State University, San Luis Obispo, California, USA*
[7]*Central China Normal University, Wuhan, China*
[8]*Centre de Calcul de l'IN2P3, Villeurbanne, Lyon, France*
[9]*Centro de Aplicaciones Tecnológicas y Desarrollo Nuclear (CEADEN), Havana, Cuba*
[10]*Centro de Investigación y de Estudios Avanzados (CINVESTAV), Mexico City and Mérida, Mexico*
[11]*Centro Fermi - Museo Storico della Fisica e Centro Studi e Ricerche "Enrico Fermi", Rome, Italy*
[12]*Chicago State University, Chicago, Illinois, United States*
[13]*China Institute of Atomic Energy, Beijing, China*
[14]*Chonbuk National University, Jeonju, Republic of Korea*
[15]*Comenius University Bratislava, Faculty of Mathematics, Physics and Informatics, Bratislava, Slovakia*
[16]*COMSATS Institute of Information Technology (CIIT), Islamabad, Pakistan*
[17]*Creighton University, Omaha, Nebraska, United States*
[18]*Department of Physics, Aligarh Muslim University, Aligarh, India*
[19]*Department of Physics, Ohio State University, Columbus, Ohio, United States*
[20]*Department of Physics, Pusan National University, Pusan, Republic of Korea*
[21]*Department of Physics, Sejong University, Seoul, Republic of Korea*

[22]*Department of Physics, University of California, Berkeley, California, United States*
[23]*Department of Physics, University of Oslo, Oslo, Norway*
[24]*Department of Physics and Technology, University of Bergen, Bergen, Norway*
[25]*Dipartimento di Fisica dell'Università "La Sapienza" and Sezione INFN, Rome, Italy*
[26]*Dipartimento di Fisica dell'Università and Sezione INFN, Cagliari, Italy*
[27]*Dipartimento di Fisica dell'Università and Sezione INFN, Trieste, Italy*
[28]*Dipartimento di Fisica dell'Università and Sezione INFN, Turin, Italy*
[29]*Dipartimento di Fisica e Astronomia dell'Università and Sezione INFN, Bologna, Italy*
[30]*Dipartimento di Fisica e Astronomia dell'Università and Sezione INFN, Catania, Italy*
[31]*Dipartimento di Fisica e Astronomia dell'Università and Sezione INFN, Padova, Italy*
[32]*Dipartimento di Fisica "E. R. Caianiello" dell'Università and Gruppo Collegato INFN, Salerno, Italy*
[33]*Dipartimento DISAT del Politecnico and Sezione INFN, Turin, Italy*
[34]*Dipartimento di Scienze e Innovazione Tecnologica dell'Università del Piemonte Orientale and INFN Sezione di Torino, Alessandria, Italy*
[35]*Dipartimento Interateneo di Fisica 'M. Merlin' and Sezione INFN, Bari, Italy*
[36]*European Organization for Nuclear Research (CERN), Geneva, Switzerland*
[37]*Faculty of Engineering and Business Administration, Western Norway University of Applied Sciences, Bergen, Norway*
[38]*Faculty of Nuclear Sciences and Physical Engineering, Czech Technical University in Prague, Prague, Czech Republic*
[39]*Faculty of Science, P. J. Šafárik University, Košice, Slovakia*
[40]*Frankfurt Institute for Advanced Studies, Johann Wolfgang Goethe-Universität Frankfurt, Frankfurt, Germany*
[41]*Gangneung-Wonju National University, Gangneung, Republic of Korea*
[42]*Gauhati University, Department of Physics, Guwahati, India*
[43]*Helmholtz-Institut für Strahlen- und Kernphysik, Rheinische Friedrich-Wilhelms-Universität Bonn, Bonn, Germany*
[44]*Helsinki Institute of Physics (HIP), Helsinki, Finland*
[45]*Hiroshima University, Hiroshima, Japan*
[46]*Hochschule Worms, Zentrum für Technologietransfer und Telekommunikation (ZTT), Worms, Germany*
[47]*Horia Hulubei National Institute of Physics and Nuclear Engineering, Bucharest, Romania*
[48]*Indian Institute of Technology Bombay (IIT), Mumbai, India*
[49]*Indian Institute of Technology Indore, Indore, India*
[50]*Indonesian Institute of Sciences, Jakarta, Indonesia*
[51]*INFN, Laboratori Nazionali di Frascati, Frascati, Italy*
[52]*INFN, Sezione di Bari, Bari, Italy*
[53]*INFN, Sezione di Bologna, Bologna, Italy*
[54]*INFN, Sezione di Cagliari, Cagliari, Italy*
[55]*INFN, Sezione di Catania, Catania, Italy*
[56]*INFN, Sezione di Padova, Padova, Italy*
[57]*INFN, Sezione di Roma, Rome, Italy*
[58]*INFN, Sezione di Torino, Turin, Italy*
[59]*INFN, Sezione di Trieste, Trieste, Italy*
[60]*Inha University, Incheon, Republic of Korea*
[61]*Institut de Physique Nucléaire d'Orsay (IPNO), Institut National de Physique Nucléaire et de Physique des Particules (IN2P3/CNRS), Université de Paris-Sud, Université Paris-Saclay, Orsay, France*
[62]*Institute for Nuclear Research, Academy of Sciences, Moscow, Russia*
[63]*Institute for Subatomic Physics of Utrecht University, Utrecht, Netherlands*
[64]*Institute for Theoretical and Experimental Physics, Moscow, Russia*
[65]*Institute of Experimental Physics, Slovak Academy of Sciences, Košice, Slovakia*
[66]*Institute of Physics, Bhubaneswar, India*
[67]*Institute of Physics of the Czech Academy of Sciences, Prague, Czech Republic*
[68]*Institute of Space Science (ISS), Bucharest, Romania*
[69]*Institut für Kernphysik, Johann Wolfgang Goethe-Universität Frankfurt, Frankfurt, Germany*
[70]*Instituto de Ciencias Nucleares, Universidad Nacional Autónoma de México, Mexico City, Mexico*
[71]*Instituto de Física, Universidade Federal do Rio Grande do Sul (UFRGS), Porto Alegre, Brazil*
[72]*Instituto de Física, Universidad Nacional Autónoma de México, Mexico City, Mexico*
[73]*iThemba LABS, National Research Foundation, Somerset West, South Africa*
[74]*Johann-Wolfgang-Goethe Universität Frankfurt Institut für Informatik, Fachbereich Informatik und Mathematik, Frankfurt, Germany*
[75]*Joint Institute for Nuclear Research (JINR), Dubna, Russia*
[76]*Konkuk University, Seoul, Republic of Korea*
[77]*Korea Institute of Science and Technology Information, Daejeon, Republic of Korea*
[78]*KTO Karatay University, Konya, Turkey*
[79]*Laboratoire de Physique Subatomique et de Cosmologie, Université Grenoble-Alpes, CNRS-IN2P3, Grenoble, France*

[80]*Lawrence Berkeley National Laboratory, Berkeley, California, USA*
[81]*Lund University Department of Physics, Division of Particle Physics, Lund, Sweden*
[82]*Nagasaki Institute of Applied Science, Nagasaki, Japan*
[83]*Nara Women's University (NWU), Nara, Japan*
[84]*National and Kapodistrian University of Athens, School of Science, Department of Physics, Athens, Greece*
[85]*National Centre for Nuclear Research, Warsaw, Poland*
[86]*National Institute of Science Education and Research, HBNI, Jatni, India*
[87]*National Nuclear Research Center, Baku, Azerbaijan*
[88]*National Research Centre Kurchatov Institute, Moscow, Russia*
[89]*Niels Bohr Institute, University of Copenhagen, Copenhagen, Denmark*
[90]*Nikhef, National institute for subatomic physics, Amsterdam, Netherlands*
[91]*NRC Kurchatov Institute IHEP, Protvino, Russia*
[92]*NRNU Moscow Engineering Physics Institute, Moscow, Russia*
[93]*Nuclear Physics Group, STFC Daresbury Laboratory, Daresbury, United Kingdom*
[94]*Nuclear Physics Institute of the Czech Academy of Sciences, Řež u Prahy, Czech Republic*
[95]*Oak Ridge National Laboratory, Oak Ridge, Tennessee, USA*
[96]*Petersburg Nuclear Physics Institute, Gatchina, Russia*
[97]*Physics department, Faculty of science, University of Zagreb, Zagreb, Croatia*
[98]*Physics Department, Panjab University, Chandigarh, India*
[99]*Physics Department, University of Jammu, Jammu, India*
[100]*Physics Department, University of Rajasthan, Jaipur, India*
[101]*Physikalisches Institut, Eberhard-Karls-Universität Tübingen, Tübingen, Germany*
[102]*Physikalisches Institut, Ruprecht-Karls-Universität Heidelberg, Heidelberg, Germany*
[103]*Physik Department, Technische Universität München, Munich, Germany*
[104]*Research Division and ExtreMe Matter Institute EMMI, GSI Helmholtzzentrum für Schwerionenforschung GmbH, Darmstadt, Germany*
[105]*Rudjer Bošković Institute, Zagreb, Croatia*
[106]*Russian Federal Nuclear Center (VNIIEF), Sarov, Russia*
[107]*Saha Institute of Nuclear Physics, Kolkata, India*
[108]*School of Physics and Astronomy, University of Birmingham, Birmingham, United Kingdom*
[109]*Sección Física, Departamento de Ciencias, Pontificia Universidad Católica del Perú, Lima, Peru*
[110]*Stefan Meyer Institut für Subatomare Physik (SMI), Vienna, Austria*
[111]*SUBATECH, IMT Atlantique, Université de Nantes, CNRS-IN2P3, Nantes, France*
[112]*Suranaree University of Technology, Nakhon Ratchasima, Thailand*
[113]*Technical University of Košice, Košice, Slovakia*
[114]*Technische Universität München, Excellence Cluster "Universe", Munich, Germany*
[115]*The Henryk Niewodniczanski Institute of Nuclear Physics, Polish Academy of Sciences, Cracow, Poland*
[116]*The University of Texas at Austin, Austin, Texas, USA*
[117]*Universidad Autónoma de Sinaloa, Culiacán, Mexico*
[118]*Universidade de São Paulo (USP), São Paulo, Brazil*
[119]*Universidade Estadual de Campinas (UNICAMP), Campinas, Brazil*
[120]*Universidade Federal do ABC, Santo Andre, Brazil*
[121]*University College of Southeast Norway, Tonsberg, Norway*
[122]*University of Cape Town, Cape Town, South Africa*
[123]*University of Houston, Houston, Texas, USA*
[124]*University of Jyväskylä, Jyväskylä, Finland*
[125]*University of Liverpool, Liverpool, United Kingdom*
[126]*University of Split, Faculty of Electrical Engineering, Mechanical Engineering and Naval Architecture, Split, Croatia*
[127]*University of Tennessee, Knoxville, Tennessee, USA*
[128]*University of the Witwatersrand, Johannesburg, South Africa*
[129]*University of Tokyo, Tokyo, Japan*
[130]*University of Tsukuba, Tsukuba, Japan*
[131]*Université Clermont Auvergne, CNRS/IN2P3, LPC, Clermont-Ferrand, France*
[132]*Université de Lyon, Université Lyon 1, CNRS/IN2P3, IPN-Lyon, Villeurbanne, Lyon, France*
[133]*Université de Strasbourg, CNRS, IPHC UMR 7178, F-67000 Strasbourg, France, Strasbourg, France*
[134]*Université Paris-Saclay Centre dÉtudes de Saclay (CEA), IRFU, Department de Physique Nucléaire (DPhN), Saclay, France*
[135]*Università degli Studi di Pavia, Pavia, Italy*
[136]*Università di Brescia, Brescia, Italy*
[137]*V. Fock Institute for Physics, St. Petersburg State University, St. Petersburg, Russia*
[138]*Variable Energy Cyclotron Centre, Kolkata, India*

[139] *Warsaw University of Technology, Warsaw, Poland*
[140] *Wayne State University, Detroit, Michigan, USA*
[141] *Westfälische Wilhelms-Universität Münster, Institut für Kernphysik, Münster, Germany*
[142] *Wigner Research Centre for Physics, Hungarian Academy of Sciences, Budapest, Hungary*
[143] *Yale University, New Haven, Connecticut, USA*
[144] *Yonsei University, Seoul, Republic of Korea*

[a]Dipartimento DET del Politecnico di Torino, Turin, Italy.
[b]M. V. Lomonosov Moscow State University, D. V. Skobeltsyn Institute of Nuclear, Physics, Moscow, Russia.
[c]Department of Applied Physics, Aligarh Muslim University, Aligarh, India.
[d]Deceased.
[e]Institute of Theoretical Physics, University of Wroclaw, Poland.